Shock metamorphism of some minerals: Basic introduction and microstructural observations

FALKO LANGENHORST

Bayerisches Geoinstitut, University of Bayreuth, Universitätsstr. 30, D-95447 Bayreuth, Germany; e-mail: Falko.Langenhorst@uni-bayreuth.de

Abstract. Minerals show a unique behaviour when subjected to shock waves. The ultradynamic loading to high pressures and temperatures causes deformation, transformation and decomposition phenomena in minerals that are unequivocal indicators of impact events. This paper introduces into the basics of shock compression, required to understand the formation and experimental calibration of these shock effects in minerals, and particularly focuses on the recent advances in the field of shock metamorphism achieved by the application of transmission electron microscopy (TEM). TEM studies underline that the way minerals respond to shock compression largely depends on their crystal structures and chemical compositions, as is illustrated here on the basis of four minerals: quartz, olivine, graphite and calcite.

The crystal structure of a mineral exerts an important control on the shock-induced deformation phenomena, comprising one- to two-dimensional lattice defects, such as dislocations, mechanical twins, planar fractures, and amorphous planar deformation lamellae. For example, dislocations cannot be activated in quartz due to the strong covalent bonding, whereas the island silicate olivine easily deforms by dislocation glide.

Transformation phenomena include phase transitions to (diaplectic) glass and/or high-pressure polymorphs. TEM studies reveal that high-pressure polymorphs such as coesite, stishovite and ringwoodite are liquidus phases, which form upon decompression by crystallization from high-pressure melts. The graphite-to-diamond transition is however a rare example for a solid-state transformation, taking place by a martensitic shear mechanism.

Shock-induced decomposition reactions are typical of volatile-bearing minerals and liberate toxic gases that, in case of large impacts, may affect Earth's climate. Shock experiments show that degassing of calcite does not take place under high pressure but can massively occur after decompression if the post-shock temperature is sufficiently high. A recombination reaction happens however if CaO and CO_2 are not physically separated.

Key words: impact features, shock metamorphism, shock waves, minerals, crystal structure, defects, experimental study

Introduction

Collisions of solid bodies played a crucial role in the formation of Earth and its subsequent evolution. The Proto-Earth accreted by collisions of planetesimals (Wetherill 1984) and underwent, in Archean times, a very heavy bombardment (Melosh 1989). The high collision rate at the beginning of Earth was simply the consequence of the chaotic states in the orbital movements of early solid bodies. Subsequently, this early collision rate distinctly declined until about 2.5 Ga, and since then we have an essentially constant flux of bodies colliding with Earth (Fig. 1).

This knowledge of the collision history of Earth is however not exclusively based on observations of terrestrial impact craters, as one would possibly expect, but it largely relies on the cratering history of the Moon (Chapman and Morrison 1994, Neukum et al. 2001, Stöffler and Ryder 2001). Due to the absence of an atmosphere (and hence weathering) and the early cessation of volcanic activity on Moon, impact craters accumulated, in nearly undisturbed fashion, particularly in the lunar highlands, where crater densities are highest. On the geologically very active Earth, the morphologic landforms of impact craters easily disappear beyond recognition due to erosion, plate tectonics and other exogenic and endogenic processes. Although four Archean impact layers have been reported (Byerly et al. 2002), we have no knowledge of an Archean crater (Fig. 2). According to the cratering statis-
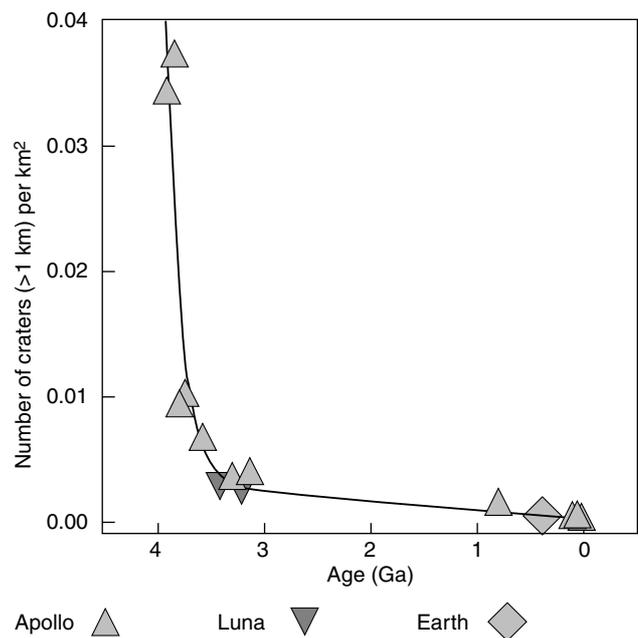

Fig. 1. Cratering statistics of the Moon-Earth system for the last 4 Ga years [data from Stöffler and Ryder (2001) and regression curve after Neukum et al. (2001)].

tics (Fig. 1), one would however expect that most craters formed during this early episode of Earth (Grieve and Shoemaker 1994).
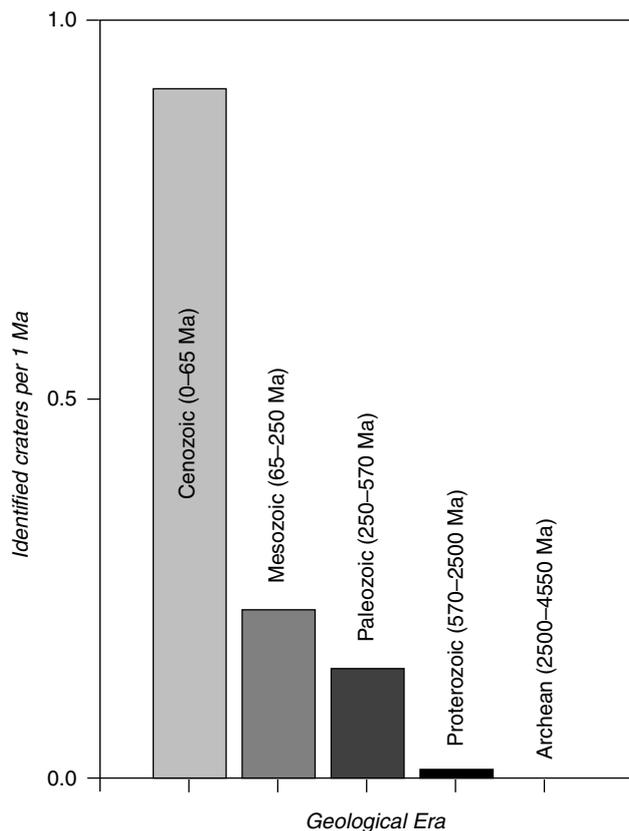
Fig. 2. The number of identified impact craters per Ma plotted for different eras in the Earth history. Note that despite the high cratering activity in the Archean we have no knowledge of an impact crater from this time period (cf. Fig. 1, data from http://gdcinfo.agg.nrcan.gc.ca/crater/world_craters_e.html).

Impact events are however not only expressed at the large scale in the form of circular craters but they manifest also at microscopic scales in minerals. This article focuses on these microscopic traces in minerals termed shock or shock-metamorphic effects. Shock effects in minerals are an unequivocal fingerprint and, often, the last remnants of impact events. Even if the crater is completely erased, shocked minerals can be preserved in distal or global ejecta horizons, still providing evidence of the impact and its age. In case of the Cretaceous/Tertiary extinction (Alvarez et al. 1980), the discovery of shocked minerals in the KT boundary layer increased, for example, the efforts to find the corresponding impact structure (Bohor et al. 1984 and 1987), subsequently identified as the Chicxulub crater (Hildebrand et al. 1991).

In the last 10–15 years we have obtained new insights and a better understanding of the shock behaviour of minerals, mainly due to the increased use of transmission electron microscopy (TEM). In terms of spatial resolution, this technique is well superior to optical microscopy. Therefore, it became possible to decipher the nature of shock phenomena already known from optical studies (e.g. planar deformation features (PDFs)), to discover so-far unknown effects, and to understand their mechanisms of

formation and subsequent alteration. This article does not aim to give a comprehensive review on shocked minerals; for a more detailed compilation the reader is referred to: e.g., French and Short (1968), Stöffler (1972, 1974), Stöffler and Langenhorst (1994), French (1998), Deutsch and Langenhorst (1998), Langenhorst and Deutsch (1998). It is merely an attempt to utilize instructive examples to explain the specific response of minerals to shock compression, which is distinctly different from the transformation and deformation behaviour of minerals in other geologic processes, principally of lower strain rate.

Principles of shock waves

From a basic understanding of shock waves it will be immediately clear why minerals respond differently to impact than to other geologic processes. It will also help to understand the mechanics of the large-scale crater-forming process (Roddy et al. 1977, Melosh 1989). A shock wave is an extreme compression wave that propagates with supersonic velocity, abruptly compresses, heats, and plastically deforms solid matter. In this respect, shock waves are fundamentally different from seismic (elastic) waves (e.g. Duvall and Fowles 1963).

A shock wave is produced by the impact of a high-velocity projectile or the detonation of an explosive (Roddy et al. 1977, Asay and Shahinpoor 1993). In these processes, the time of load is extremely short and, therefore, the initial stress wave steepens immediately to an almost atomically sharp discontinuity, which separates highly compressed from uncompressed material. This so-called "shock front" represents consequently an infinite discontinuity in all state parameters (Duvall and Fowles 1963, Melosh 1989): pressure P, temperature T, specific volume V, and energy E. Minerals and rocks undergo some kind of a physical "shock", because they have to instantly adapt to extreme P,T conditions with strain rates on the order of 10^6 to 10^9 s^{-1}. Additionally, a shock wave is very short-lived with a typical pulse duration of about 1 second for a natural impact of a 10 km diameter projectile. It is due to these two time parameters, high strain rates and short shock duration, that minerals cannot respond by equilibrium reactions but rather by the activation of fast deformation and transformation mechanisms.

The unusual properties of shock waves can be illustrated by a simple train model (Fig. 3). The cartoon shows the collision of a moving train (projectile) with a standing train (target). The collision leads to deformation and compression of the hitting locomotive and the wagons in two opposite directions. The two boundaries between compressed and uncompressed wagons are the shock fronts, which propagate with the shock velocity U. An additional effect of the compression is material flow in the direction of the target (see the displacement of the boundary between the hitting locomotive and the last target wagon). The material moves behind the shock wave into the target,

at a particle velocity u_p, which is distinctly smaller than the shock velocity U. As the process proceeds, more and more wagons are engulfed by the compression until the shock wave in the projectile is reflected as rarefaction wave at the free rear side of the projectile (Fig. 3). This leads to a backward acceleration of wagons and represents the ejection of material in natural impact cratering. As the rarefaction wave is propagating in already compressed material, it is faster than the shock wave in the target. Consequently, the shock wave will be overtaken at some depth by the rarefaction wave, i.e. it will decay.

Both shock U and particle u_p velocities characterise the state of material under shock compression and are related to pressure P, density ρ, and energy E via the Hugoniot equations (Duvall and Fowles 1963, Melosh 1989):

$$\rho_0 U = \rho (U - u_p) \qquad (1)$$
$$P - P_0 = \rho_0 U u_p \qquad (2)$$
$$P u_p = \rho_0 U (u_p^2/2) + \rho_0 U (E - E_0) \qquad (3)$$

These equations express the conservation of mass, momentum, and energy across the shock front. By combining equations *(1)* to *(3)* the velocities can be eliminated to give the so-called Rankine-Hugoniot equation:

$$E - E_0 = (P - P_0) (V_0 - V)/2 \qquad \text{with } V = 1/\rho \quad (4)$$

This is an equation of state, describing the physical states that can be achieved by shock waves of variable intensity in any solid. Commonly, the shock equation of state of a particular material is experimentally determined by measuring particle u_p and shock U velocities. Since the zero-pressure densities ρ_0 of minerals are usually well known, pressures P and densities ρ (or specific volumes V) can be calculated with the above mentioned Hugoniot equations.

As is usual for all equations of state, the shock data of a particular material are displayed in a pressure-specific volume plot, defining the so-called Hugoniot curve. The Hugoniot curves of rock-forming minerals are commonly characterised by kinks, i.e., discontinuous changes in the curve slope. One discontinuity is typically at 5–10 GPa, the so-called Hugoniot elastic limit, which is the yield strength of the material. Discontinuities at higher pressures were generally assumed to result from phase transformations to high-pressure polymorphs (e.g. Ahrens and Rosenberg 1968, Jackson and Ahrens 1979, Ahrens et al. 1976, Melosh 1989). This interpretation is certainly correct for materials such as iron and graphite, which undergo martensitic (displacive) transformations, fast enough to take place under shock compression. It is however an inappropriate assumption for silicate materials such as quartz, feldspars and olivine. These minerals can only be converted into high-pressure polymorphs via reconstructive mechanisms. These mechanisms are however too time-consuming to occur under shock compression. Therefore, shock experiments on these minerals usually result in the formation of dense (diaplectic) glass with possibly five- and/or six-fold coordinated silicon or finely recrystallised low-pressure phase.
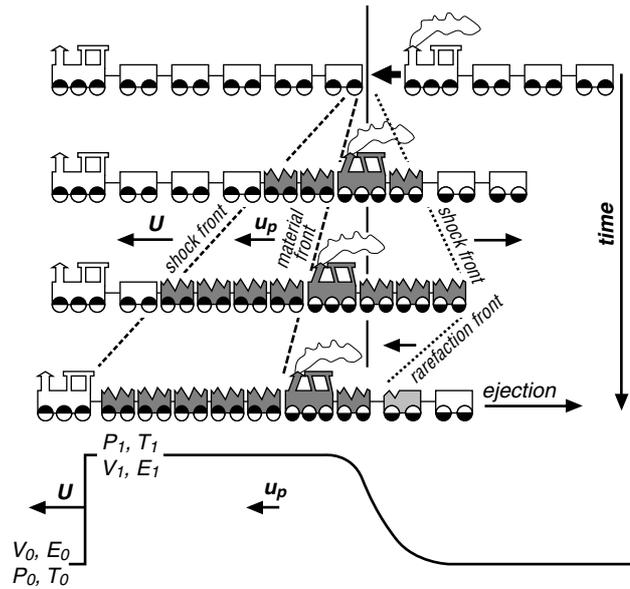

Fig. 3. A train model illustrating the formation and propagation of shock and rarefaction waves and the associated material movement (from Langenhorst 2000).

Experimental simulation

Shock experiments are indispensable for understanding the formation of shock effects in minerals, because they are performed under controlled laboratory conditions and because they provide shocked minerals in their initial, unmodified state. This has two basic advantages. First, shock effects can be calibrated as function of pressure (or other factors) and the resultant barometers can then, with some care, be applied to nature (Stöffler and Langenhorst 1994). Secondly, the study of pristine shock effects helps to understand possible post-shock modifications (annealing, chemical alteration etc.) in the natural impact environment (Grieve et al. 1996).

The major disadvantage of shock experiments is their short pulse duration (< 1μs), which is at least 6 orders of magnitude shorter than the pressure pulse in a natural bolide impact (~ 1 s, Langenhorst et al. 2002a). The short pulse duration in an experiment is simply the result of the small size of the projectile. The pressure duration corresponds approximately to the time that a shock wave needs to travel through the projectile and back (i.e. 2 projectile diameters, Fig. 3).

It may be some surprise, but pioneering, experimental work on impact processes started with Alfred Wegener (1921), the founder of plate tectonics. He simulated impact events by throwing cement powder in a tablespoon with his bare hand onto a target, which was also composed of cement powder. He was able to produce circular craters with central uplifts, resembling in shape and proportions those observed on the Moon. Since then, a large variety of sophisticated shock techniques has been developed to simulate cratering mechanics and shock metamorphism of
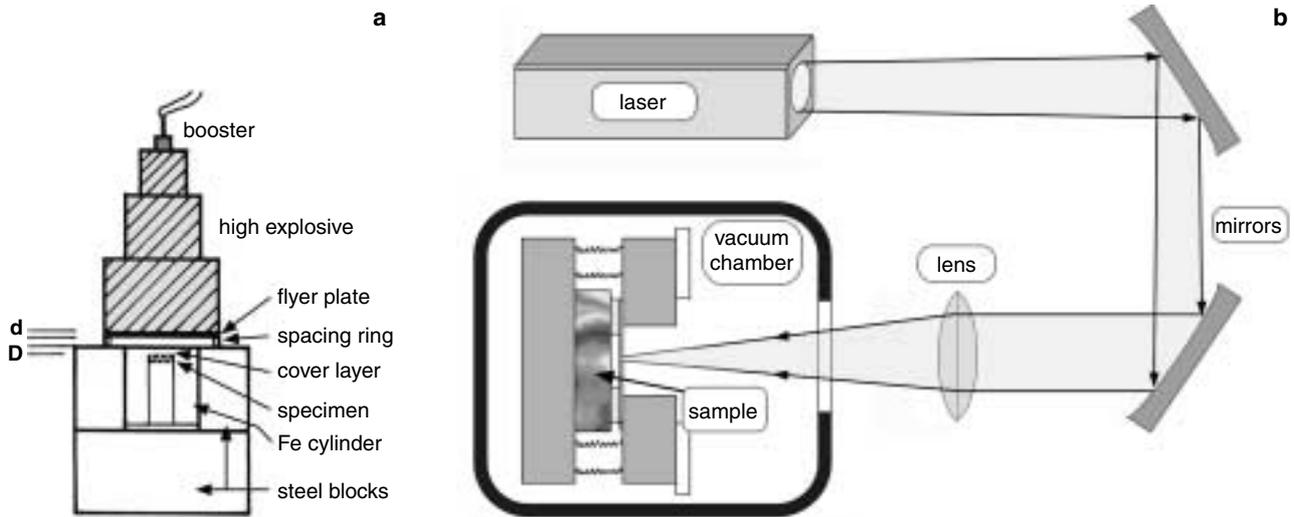
Fig. 4. Two different experimental designs to produce shock waves: (a) High-explosive device used at the Ernst-Mach-Institut, Efringen-Kirchen, Germany (modified after Langenhorst and Deutsch 1994) and (b) a laser irradiation setup with the sample being clamped into an Al block. The laser is focused on a thin Al foil, acting as flyer plate (modified after Langenhorst et al. 1999a and 2002a).

minerals (e.g. French and Short 1968, Roddy et al. 1977, Asay and Shahinpoor 1993, Davison et al. 2002).

Most experiments related to cratering mechanics employ spherical projectiles that produce and excavate some crater in an infinite half space medium via a spherically expanding shock wave. In contrast, most experiments related to shock metamorphism employ flat-plate projectiles that drive a planar shock wave through a similarly planar target; the thickness of the latter is typically less than projectile thickness to avoid measurable pressure decay across the sample (Barker et al. 1993). The target is usually a metallic container, encapsulating the sample in a fashion to allow its partial or complete recovery. The experiments may differ widely in the type of accelerating system (Fig. 4): powder and light-gas guns, high-explosive charges, electric discharge guns, and laser irradiation techniques have been used and tested to successfully reproduce shock effects in minerals (e.g. Milton and DeCarli 1963, Müller and Hornemann 1969, Gratz et al. 1992, Stöffler and Langenhorst 1994, Langenhorst et al. 1999a, 2002a). The principle of the electric gun is to vaporise a thin metal foil by rapid electric discharge of a capacitor. The high electrical current leads to the instantaneous vaporisation of the foil and the production of a shock wave (Langenhorst et al. 2002a). Laser irradiation experiments can be performed either with or without a projectile. In the latter case, the beam is directly focused on the sample surface (Langenhorst et al. 2002a), whereby the absorption of the laser energy generates rapidly exploding plasma that subsequently induces a shock wave. Such plasma techniques are capable to produce the highest shock pressures with an unbelievable world record of 750 Mbar (Cauble et al. 1993). However, higher shock pressures are commonly at the expense of shorter shock durations and smaller sample volumes. This is because higher impact velocities and hence higher shock pressures can only be achieved by re-

ducing the size and weight of the projectile. Typical pressure pulses in laser irradiation, electric discharge and high-explosive experiments are approximately 1 ns, 10 ns, and 1 μs with shocked sample volumes on the order of 0.1, 1, and 100 mm^3, respectively (Langenhorst et al. 2002a).

To determine pressures in shock experiments it is necessary to measure the velocities associated with the shock waves (projectile v, particle u and shock U velocities), using electrical pin contact, optical interferometry (VISAR) or similar techniques (Hornemann and Müller 1971, Barker et al. 1993). It is then possible to calculate the pressures
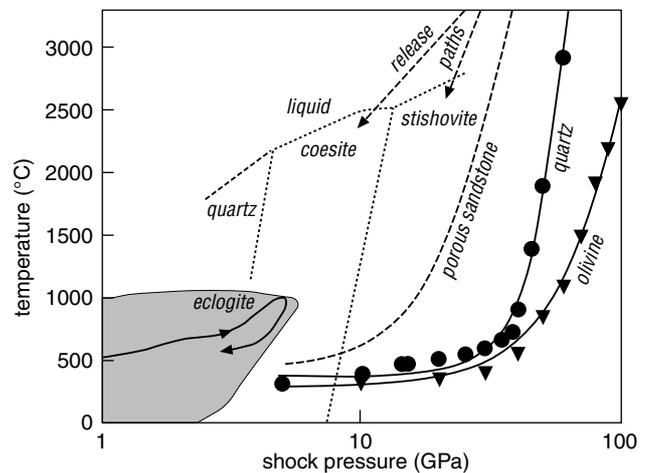

Fig. 5. Phase diagram depicting the pressure-temperature conditions reached in quartz, olivine (solid line), and porous sandstone (long dashed line) by shock compression (data after Wackerle 1962, Kieffer et al. 1976, and Holland and Ahrens 1997). The release paths hold for porous quartz, which first melts on loading and then solidifies on cooling as coesite or stishovite. The equilibrium phase boundaries between quartz, coesite, stishovite and liquid are drawn as dashed lines. The grey pressure-temperature field represents the conditions reached in regional metamorphism; the solid line within this field depicts the pressure-temperature path of a diamond-bearing gneiss (Stöckhert et al. 2001).

by aid of the known Hugoniot relations of the materials involved (Marsh 1980). Thus, the determination of shock pressure is fundamentally different from the approach used in static compression techniques (e.g. piston cylinder, multi-anvil or diamond anvil cell experiments), in which the pressures are calibrated via properties and/or phase transformations of reference materials (e.g. Rubie 1999).

The determination of temperatures is a less precise and more difficult undertaking. So far, pyrospectrometric techniques have been used to measure both shock and post-shock temperatures (e.g. Raikes and Ahrens 1979, Holland and Ahrens 1997; Fig. 5). The knowledge of temperatures is however of fundamental importance for the determination of the melting temperatures of materials at very high pressures. For example, the precise measurement of the melting curve of iron enables the temperature at the boundary between Earth's inner (solid) and outer (liquid) core to be determined (Brown and McQueen 1986), an important fix point of the geotherm.

Shock effects in minerals

Shock-induced physical and chemical changes in minerals are collectively called shock effects or shock-metamorphic effects. This term is relatively broad and covers any type of shock-induced change, such as formation of lattice defects, phase transformations, decomposition reactions and resultant changes in physical and chemical properties. A great diversity of natural shock effects has been described on the basis of spectroscopic techniques, X-ray diffraction, and optical microscopy (Hörz and Quaide 1973, Stöffler 1972 and 1974, Schneider 1978, Boslough et al. 1989). The physical nature of some of the effects was not completely clear and others were not even known until TEM was used to characterize the mineralogical effects at the nanometer scale. Based on TEM observations, the following simple subdivision of shock effects and processes occurring during shock compression and decompression has been proposed (Langenhorst and Deutsch 1998):

(1) **Deformation**: formation of dislocations, planar microstructures (planar fractures and planar deformation features), mechanical twins, kink bands, and mosaicism

(2) **Phase transformations** into high-pressure phases and diaplectic glass

(3) **Decomposition** into a solid residue and a gaseous phase

(4) **Melting** and **vaporisation** of entire mineral (subsequently quenched as shock-fused glass or polycrystalline aggregates)

This simple list does not contain the post-shock thermal effects forming distinctly after the impact. In a wide sense, these effects may also be regarded as shock indicators, although they are not primary effects of shock compression and decompression and simply result from the high temperatures prevailing after an impact event. Exam-
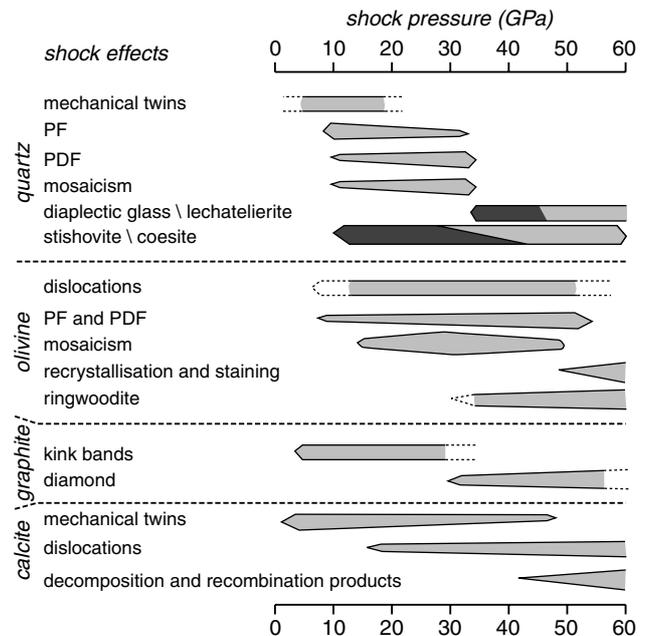

Fig. 6. Compilation of the pressure intervals over which certain shock effects are formed in quartz, olivine, graphite and calcite (modified after Stöffler and Langenhorst 1994 and Langenhorst and Deutsch 1998). The diagram is based on shock experiments with non-porous samples.

ples of diagnostic post-shock effects are the formation of Ballen quartz and checkerboard feldspars in impact melts (Carstens 1975, Bischoff and Stöffler 1984) or the crystallization of highly oxidised Ni-rich spinels (magnesioferrites) in microtektites (Robin et al. 1992).

We will focus here exclusively on the shock effects listed above. The deformation and transformation effects largely form during the compression phase of shock waves, whereas decomposition, melting and vaporisation are temperature dominated processes, which take place during the decompression phase when pressure declines to a larger extent than temperature. There is no single mineral that shows all of these effects (Fig. 6). The response of a mineral to shock compression largely depends on its crystal structure and composition. A mineral with strong three-dimensional covalent bonding between polyhedra in the crystal structure can, for example, not respond by dislocation glide. Also, minerals without volatile components cannot respond by decomposition reactions such as dehydration and decarbonation. To highlight these aspects and to illustrate the various types of shock effects in minerals we will concentrate on four minerals, differing largely in terms of crystal structure and composition.

Quartz

Among the rock-forming minerals, quartz (SiO_2) displays the widest variety of shock effects. It possesses a crystal structure, consisting of three-dimensionally linked, corner-shared SiO_4-tetrahedra with strong covalent bonding. In the low-pressure regime (< 30 GPa), quartz can
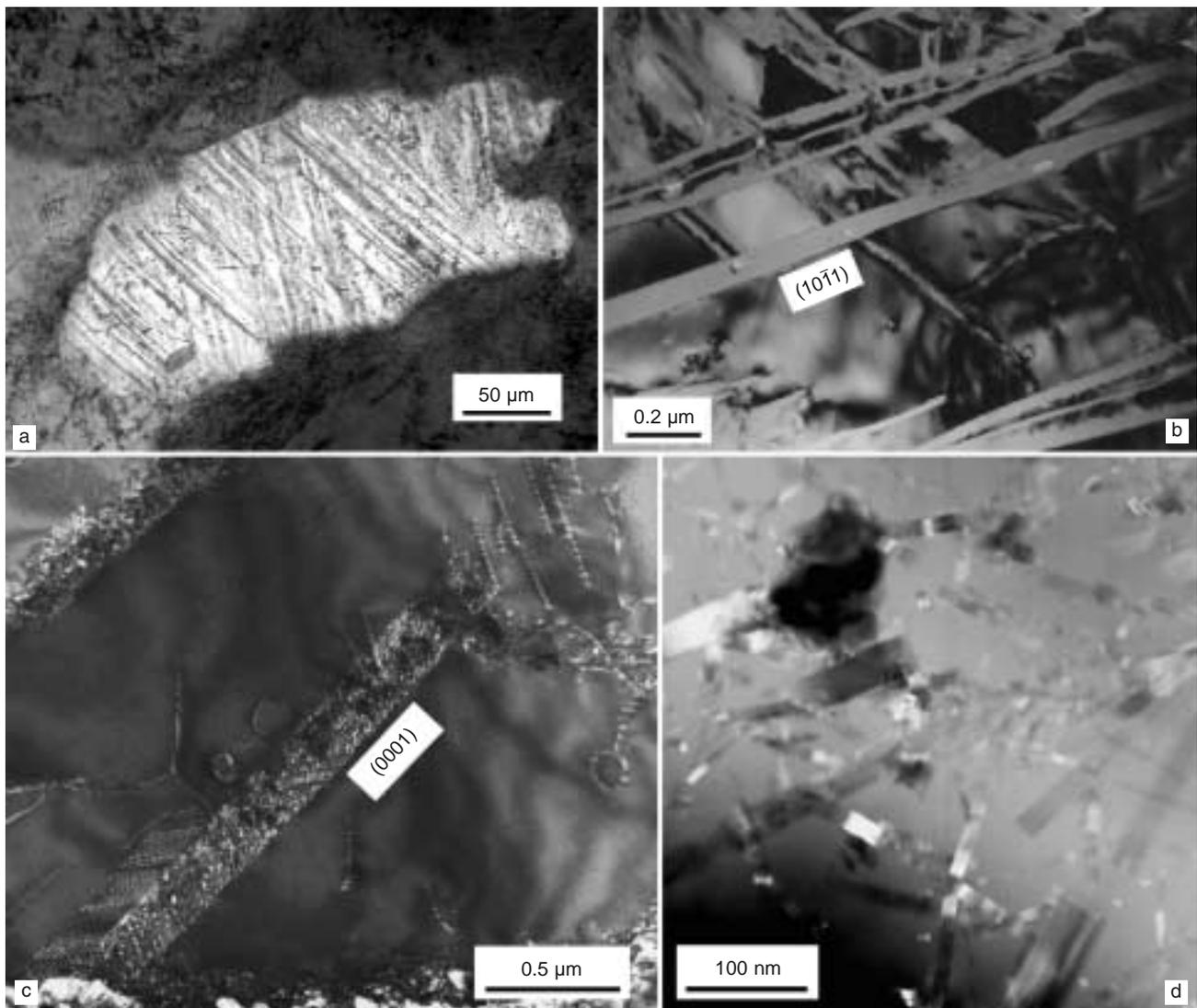
Fig. 7. Shock effects in quartz: (a) Optical micrograph of planar deformation features in shocked quartz in a garnet gneiss from the Popigai crater, Siberia, (b) bright-field TEM image of fresh, amorphous PDFs in shocked quartz from the Massignano outcrop, Italy (see Langenhorst 1996), (c) Dark-field TEM image of a mechanical Brazil twin in shocked quartz from the Mjølnir crater, Barents Sea and (d) dark-field scanning TEM image of numerous stishovite needles embedded in a glassy shock vein of the Zagami meteorite (see Langenhorst and Poirier 2000).

therefore not react by dislocation glide, particularly because the activation and glide of dislocations is controlled by the diffusion of water-related defects (see McLaren 1991 for "*hydrolytic weakening*"), which is a rather slow process compared to the short time frame of shock compression.

Instead, quartz develops so-called planar microstructures (Grieve et al. 1990), which comprise planar fractures (PF), planar deformation features (PDFs), and mechanical twins (Stöffler and Langenhorst 1994). The mechanical twins were previously also regarded as PDFs, because a distinction on the basis of optical microscopy is impossible.

PFs can basically be regarded as high-pressure cleavage planes that are only activated by dynamic shock loading; they are relatively widely spaced (> 5–20 μm). On the contrary, quartz has no cleavage at ambient conditions and fails by a glassy-like parting.

PDFs were previously also called planar elements (Engelhardt and Bertsch 1969) and are thin (< 200–300 nm) amorphous lamellae with the same composition as the host crystal (Fig. 7b); at the TEM scale, their spacing (< 1 μm) is much smaller than that of PFs (Müller 1969, Ashworth and Schneider 1985, Gratz et al. 1992, Langenhorst 1994). PDF orientations are crystallographically controlled and show a pressure-dependent variation. Most PDFs are oriented parallel to rhombohedral planes such as {10$\bar{1}$3} and {10$\bar{1}$2}; other less abundant PDF orientations are given in Table 1 (see also Stöffler and Langenhorst 1994). In the low-pressure regime (< 30 GPa), PDF orientations are regarded as the most robust barometer, because even post-shock annealing and alteration merely converts the PDFs into the "decorated" type (French 1969; Fig. 7a), but PDF orientations remain unchanged. The decoration of PDFs in naturally shocked quartz is due to recrystallization of the

amorphous lamellae and resultant exsolution of water. The exsolution of water can be attributed to the different solubility of water in silica glass and crystalline quartz. Therefore, the fluids mobilized in impact events can initially be dissolved in the amorphous PDFs but subsequent recrystallization of the glass expels the water in form of tiny voids (Goltrant et al. 1991, 1992, Leroux and Doukhan 1996, Grieve et al. 1996, Langenhorst and Deutsch 1998).

Sub-planar features of tectonic origin such as the so-called Böhm lamellae have been erroneously assigned as PDFs (Ernstson et al. 1985, Vrána 1987; Fig. 8a). TEM studies have deciphered the nature of these tectonic features, as being subgrain boundaries (Cordier et al. 1994, Langenhorst and Deutsch 1996, Joreau et al. 1997a). Subgrain boundaries are dislocation arrays, separating a crystal into sub-grains that are slightly tilted (< 5°) with respect to each other. They are the result of slow plastic deformation and recovery of deformed quartz in a tectonic environment. The deformation proceeds by the activation and emission of dislocations coupled with simultaneous or subsequent climb and recovery of dislocations into sub-grain boundaries (Fig. 8b; Poirier 1985). Water can easily penetrate along these internal boundaries leading to a decoration with water bubbles.

A careful optical inspection of the suspected planar features in quartz will immediately reveal whether they are of endogenic or exogenic origin. Sub-grain boundaries show a sub-parallel arrangement but are not perfectly planar, unlike shock-produced PDFs. The spacing of tectonic features (usually > 5–10 μm) is larger than that of shock-produced PDFs (< 1 μm). Under crossed Nicols, the tec-

tonically deformed quartz grains show undulatory extinction and can exhibit an anomalous optic axial angle of up to 10°. In contrast, shocked quartz usually shows a patchy extinction pattern, with extinct areas in different parts of the crystal. This behaviour is the so-called mosaicism. In a tectonic source rock, not all of the deformed quartz grains contain sub-grain boundaries in a sub-planar arrangement; many quartz grains may even be devoid of sub-grain boundaries. On the other hand, it would be rather unusual for an impact rock that only one or few quartz grains contain PDFs. If the quartz grains have experienced the same pressure-temperature conditions, then at least most of them should contain PDFs (Hörz 1968, Engelhardt and Bertsch 1969). The size and orientation of quartz grains with respect to the shock front has however an influence on the development of PDFs (Walzebuck and Engelhardt

Table 1. Compilation of the most abundant PDF orientations in shocked quartz.

Miller indices {h k i l}	Azimuth angle	Pole distance ρ	Symbol	Form
(0001)	–	0°	c	basal pinacoid
{10$\bar{1}$3}, {01$\bar{1}$3} p, n	30°	22.95°	ω, ω'	rhombohedron
{10$\bar{1}$2}, {01$\bar{1}$2} p, n	30°	32.42°	π, π'	rhombohedron
{10$\bar{1}$1}, {01$\bar{1}$1} p, n	30°	51.79°	r, z	rhombohedron
{10$\bar{1}$0}	30°	90°	m	hexagonal prism
{40$\bar{4}$1}v, {04$\bar{4}$1} p, n	30°	78.87°	t	rhombohedron
{5$\bar{1}$60}, {6$\bar{1}$50} r, l	40°	90°	k	ditrigonal prism
{5$\bar{1}$61}, {6$\bar{1}$51} p, n, r, l {6$\bar{1}$51}, {15$\bar{6}$1}	40°	82.07°	x	trigonal trapezoedron
{31$\bar{4}$1}, {43$\bar{1}$1} p, n, r, l {41$\bar{3}$1}, {13$\bar{4}$1}	45°	77.91°	–	trigonal trapezoedron
{21$\bar{3}$1}, {32$\bar{1}$1} p, n, r, l {31$\bar{2}$1}, {12$\bar{3}$1}	50°	73.71°	–	trigonal trapezoedron
{11$\bar{2}$2}, {2$\bar{1}\bar{1}$2} r, l	60°	47.73°	ξ	trigonal dipyramid
{11$\bar{2}$1}, {2$\bar{1}\bar{1}$1} r, l	60°	65.56°	s	trigonal dipyramid
{11$\bar{2}$0}, {2$\bar{1}\bar{1}$0} r, l	60°	90.0°	a	trigonal prism
{22$\bar{4}$1}, {4$\bar{2}\bar{2}$1} r, l	60°	77.20°		trigonal dipyramid

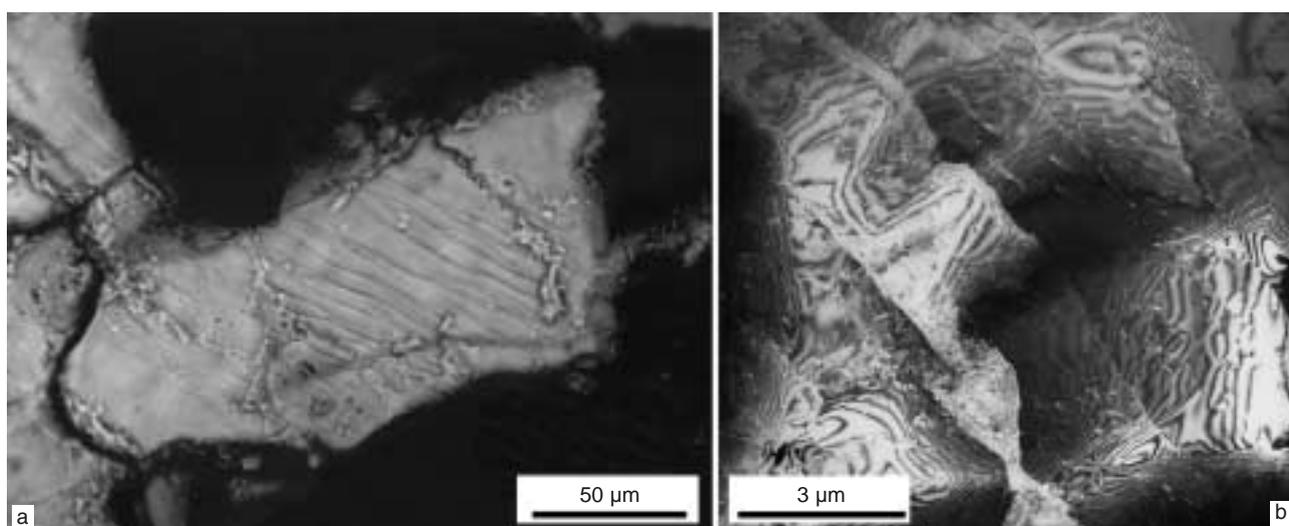p = positive, n = negative, r = right, l = left

Fig. 8. (a) Optical micrograph and (b) corresponding bright-field TEM image of subgrain boundaries in a tectonically deformed quartz from Azuara, Spain (see Langenhorst and Deutsch 1996).

50 μm

3 μm

a

b

1979). These effects may therefore be responsible for a heterogeneous PDF distribution throughout quartzose rocks, particularly at pressures required for incipient PDF formation (~ 10 GPa).

Another important outcome of TEM studies was the discovery of mechanical Brazil twins (Leroux et al. 1994), which are exclusively oriented parallel to the basal plane (0001). Numerous partial dislocations in the twin boundaries indicate the mechanical nature of the twins (Fig. 7c). In contrast, the commonly known Brazil twins are hydrothermally grown twins, which lack partial dislocations and are always oriented parallel to $(10\bar{1}1)$ (McLaren and Pithkethly 1982, Langenhorst and Poirier 2002). Static deformation experiments have shown that a high shear stress of 3 to 4 GPa has to be applied to generate the mechanical Brazil twins parallel to (0001) (McLaren et al. 1967). In crustal rocks, such conditions are only met by an impact event. At the optical scale, the mechanical twins become only visible if they are decorated with water bubbles. The mechanical Brazil twins are more resistant to post-shock annealing and alteration. Long-term regional metamorphism with complete recrystallization of the shocked rock or melting is probably the only way to erase them. At the Vredefort structure, most of the PDFs in shocked quartz are lost by post-shock overprint but the Brazil twins are still present. This discovery could explain why the PDF orientations indicate an apparent decrease in shock pressure toward the center of the crater (Schreyer 1983, Nicolaysen and Reimold 1990).

In the high-pressure regime (> 25–30 GPa), quartz is dominated by phase transformations either to diaplectic glass or to high-pressure polymorphs. Diaplectic glass is a densified glass, preserving the shape and sometimes even internal features of precursor grains (Engelhardt et al. 1967, Stöffler 1984). X-ray studies demonstrate that the transition from crystalline quartz to diaplectic glass is marked by increasing mosaicism coupled with decreasing domain size (Dachille et al. 1968, Hörz and Quaide 1973, Hanns et al. 1978). The transition is also characterized by a decrease of refractive indices and densities but diaplectic glass has a density about 5% higher than that of synthetic silica glass (Langenhorst and Deutsch 1994). It is still not fully understood on whether the transformation represents a solid-state collapse (Stöffler 1984) or quenching of a liquid under high pressure (Langenhorst 1994). The latter seems to be more likely because diaplectic glass is often associated with coesite that crystallized from high-pressure melt (see below).

Solid-state phase transformations of quartz into the high-pressure polymorphs coesite and stishovite are reconstructive. This means that time is needed for the cooperative movement and diffusion of atoms. Consequently, the short duration of shock compression impedes a direct solid-state transformation of quartz into the high-pressure polymorphs. Instead, quartz has to be melted under high pressure and the high-pressure phases can then readily crystallize during the decompression phase (see release paths in Fig. 5). The latter means that coesite and stishovite form in their stability fields at pressures, which are smaller than the maximum shock pressure achieved during the compression phase. The very high temperatures needed for melting are reached locally within shocked rocks, e.g. at pores or along shock veins, which result from shear-induced frictional melting (Kieffer et al. 1976, Langenhorst and Poirier 2000). The crystallization of high-pressure polymorphs from melt is much faster than a reconstructive solid-state transformation because the liquidus temperatures at high pressures are well above 2000°C, where kinetics is very fast. Furthermore, it is known from NMR studies that compressed silicate melts contain five- and six-fold coordinated silicon (Xue et al. 1989, Stebbins and Poe 1999), which should facilitate *per se* the crystallization of high-pressure polymorphs from such dense melts. Indeed, coesite and stishovite have always been found in conjunction with silica or rock glass (Kieffer et al. 1976, White 1993, Leroux et al. 1994, Langenhorst and Poirier 2000). Polycrystalline coesite aggregates occur in diaplectic silica glass (Hörz 1965, Stöffler 1971), e.g. at the Ries and Popigai craters. The rapid crystallization led to the formation of numerous (100) rotation twins with the composition plane (010) (Leroux et al. 1994, Grieve et al. 1996). These twins are known to represent growth defects (Bourret et al. 1986). Stishovite has been identified in the porous Coconino sandstone from the Barringer crater (Kieffer et al. 1976), in thin pseudotachylite veins in shocked basement rocks of the Vredefort structure, South Africa (Martini 1991, White 1993), as well as in shock veins in the Martian meteorite Zagami (Fig. 7d, Langenhorst and Poirier 2000). Recently, the discovery of post-stishovite polymorphs has been reported, as well (ElGoresy et al. 2000), but the high beam sensitivity prevented a thorough characterization of the phases (Sharp et al. 1999).

Olivine

Olivine is an island silicate with isolated SiO_4 tetrahedra that are joined by divalent cations. As a consequence, it is easier than in quartz to break bonds and to activate and move dislocations in this crystal structure. In the low-pressure regime, olivine deforms thus by dislocation glide. The Burgers vector b is always [001] (= c) but depending on the orientation of the olivine to the shock front, various slip planes can be activated, all sharing the c direction as zone axis (Fig. 9a): (010), (100), (110), (hk0) and symmetrically equivalent planes (Ashworth and Barber 1975, Langenhorst et al. 1995, Leroux et al. 1996, Joreau et al. 1997b, Langenhorst and Greshake 1999). The dislocation densities can be as high as 2×10^{14} m^{-2} (Madon and Poirier 1983, Langenhorst et al. 1995, Leroux 2001), even in experimentally shocked olivine (Langenhorst et al. 1999a and 2002b). Experiments have also demonstrated that dislocations can propagate at approximately half the sound velocity (~ 3 km/s, Langenhorst et al. 1999a) and are
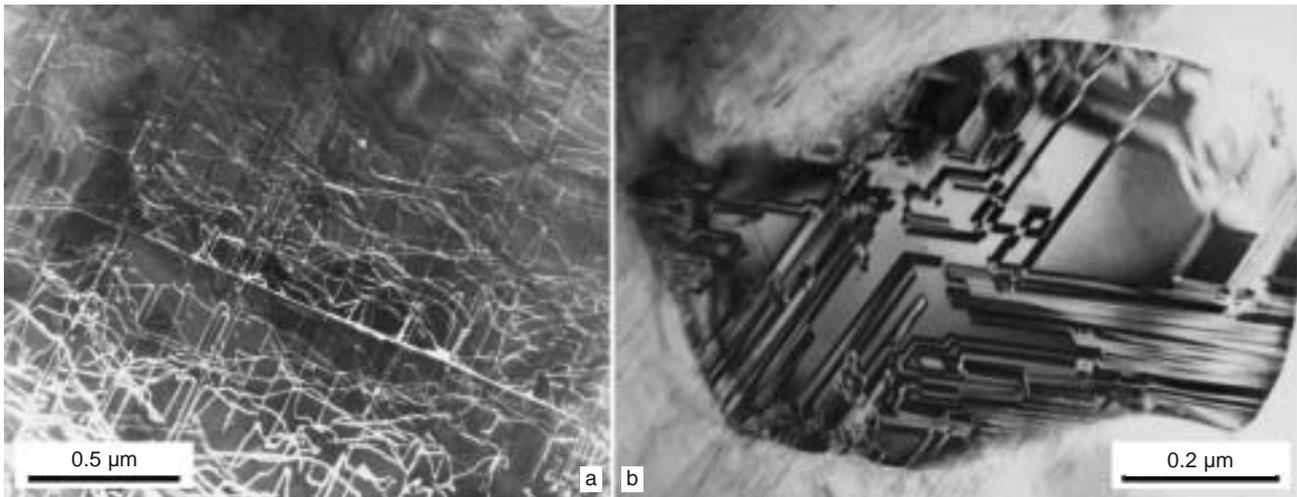
Fig. 9. (a) Dark-field TEM image of numerous *c* dislocations and a planar fracture in a shocked olivine grain from the Tenham chondrite, (b) Bright-field TEM image of ringwoodite in a shock vein of the ordinary chondrite Acfer 90072. Note the numerous stacking faults parallel to {110} planes.

probably hampered to reach this maximum speed due to interactions between themselves. The sources of dislocations seem to be the tips of forming planar fractures. When the planar fractures are formed, a high stress field is created at their tips, from which the dislocations are first emitted as loops. Since the edge component is distinctly faster than the screw component, the dislocations become very straight during further propagation, with the long dislocation line representing the screw segment.

The PFs in olivine are indicative of shock as they are oriented parallel to rational crystallographic planes that are not known as normal cleavage planes of olivine. The PFs are typically parallel to low index planes (Müller and Hornemann 1969, Snee and Ahrens 1975, Reimold and Stöffler 1978, Bauer 1979, Langenhorst et al. 1995, Stöffler et al. 1991): (100), (010), (001), (130), and (110), belonging to pinacoidal and prismatic forms. Both, the internal fragmentation of olivine by fracturing and the high density of dislocations contribute to the patchy extinction behaviour under crossed Nicols, known as mosaicism.

Observations on naturally and experimentally shocked olivine reveal that mosaicism increases distinctly in the high-pressure regime (> 25–30 GPa; Carter et al. 1968, Müller and Hornemann 1969, Snee and Ahrens 1975, Reimold and Stöffler 1978, Bauer 1979, Schmitt 2000). Additional shock phenomena in this pressure regime are staining, recrystallization, and transformation into the high-pressure polymorphs wadsleyite and ringwoodite (Fig. 9b). Although the production of glass has been reported in one experimental study (Jeanloz et al. 1977), diaplectic or shock-fused glasses are generally unknown for olivine.

Brownish staining of olivine has been described for experimentally and naturally shocked olivine (Stöffler et al. 1991, Schmitt 2000) but the reason for the colorization is unknown; a careful microstructural characterization is certainly required to unravel the nature of the staining effect.

The term recrystallisation decribes the formation of fine-grained olivine (1–2 μm) aggregates, mostly in the vicinity of shock veins. Shock-induced recrystallisation of olivine is generally assumed to be a solid-state process (Carter et al. 1968, Ashworth and Barber 1975, Bauer 1979, Stöffler et al. 1991). This interpretation actually makes sense, because recovery and polygonization of dislocations are expected to occur at elevated post-shock temperatures, resulting in fine-grained strain-free olivine aggregates with lattice-preferred orientation of subgrains (Lally et al. 1976).

In analogy to quartz, the high-pressure transformations require first the production of an olivine melt, which has then to rapidly crystallize upon decompression as high-pressure polymorphs. Such rapid crystallization is so far only manifested in shock veins of ordinary chondrites, i.e. in thin localized melt zones that are first formed by shear-induced frictional heating (Stöffler et al. 1991) and are then rapidly quenched by the surrounding cold host rock.

The shock veins contain aggregates of tiny (~1 μm) wadsleyite and ringwoodite grains, together with other high-pressure phases (Binns et al. 1969, Putnis and Price 1979, Madon and Poirier 1983, Langenhorst et al. 1995, Chen et al. 1996). Olivine melt crystallizing at pressures beyond the ringwoodite stability field yields for example an assemblage of silicate perovskite and magnesiowüstite (Sharp et al. 1997, Tomioka and Fujino 1997), the expected mineral assemblage in the Earth's lower mantle. The coexistence of high-pressure phases that should not coexist under equilibrium indicates that the crystallization of shock veins probably happened during decompression, i.e. the phases crystallized progressively from the melt while the pressure declined.

In ordinary chondrites, wadsleyite and ringwoodite are both characterized by numerous stacking faults. Wadsleyite develops faults parallel to the (010) plane (Madon and Poirier 1983) and ringwoodite parallel to {110} planes (Fig. 9b; Langenhorst et al. 1995, Chen et al. 1996). The
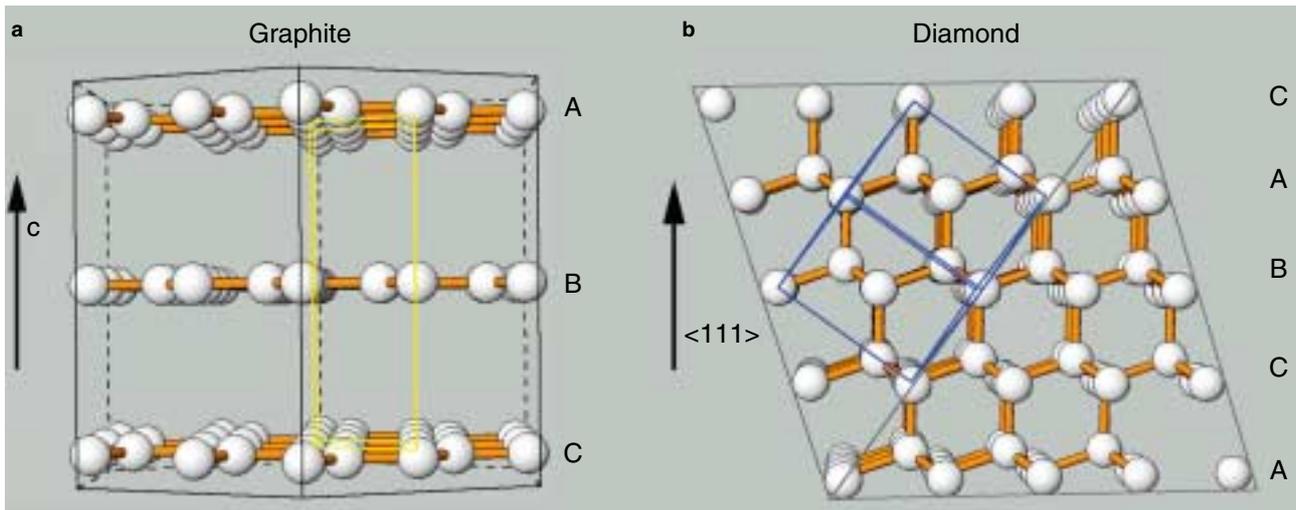
Fig. 10. Crystal structures of (a) hexagonal (ABAB…) graphite and (b) cubic (ABCABC…) diamond showing the different stacking sequences in the [0001] and [111] directions, respectively.

stacking faults are regarded as growth defects, i.e. they are an inevitable result of the short crystallization times. The time for crystallisation of shock veins depends primarily on the thickness of the vein and the initial temperature difference between vein and adjacent cold host rock. Recent calculations suggest that the times for crystallisation of high-pressure polymorphs are much shorter than the shock duration (Langenhorst and Poirier 2000).

In terrestrial impact rocks, the high-pressure polymorphs of olivine have not been found yet, probably because of the lack of well-preserved, olivine-rich target rocks with thin shock veins.

Graphite

Graphite is composed of pure carbon and is an example of a mineral with a pronounced sheet structure (Fig. 10a). Within the sheets, carbon atoms form hexagonal rings with very strong covalent bonds. Weak van-der-Waals bonding prevails between the sheets. For such a layered structure, it is characteristic to react to shock compression by kink or twin operations. In the low-pressure regime (< 25–30 GPa), graphite is usually assumed to kink but there are no exact measurements of rotation angles between different parts of shock-folded graphite crystals to exclude the possibility of twin operations (Stöffler 1972).

Graphite is of most interest for its phase transformation to diamond. In the context of impact events, the formation of diamond is a rare example for a solid-state transformation. Another mineralogical example for such a transformation is the conversion of zircon into the scheelite structured high-pressure polymorph reidite (Glass et al. 2002). Two atomic operations are necessary to convert graphite into diamond (Fig. 10). The hexagonal carbon layers have to be brought together by compression along the *c* axis and the stacking sequence has to be changed from a hexagonal to a cubic array by shearing of the

hexagonal carbon layers in their *a-a* plane. Neglecting the van-der-Waals bonds, it is not necessary to break any strong bonds within the layers. Such shear-induced transitions are called martensitic transformations. Even in short shock experiments it is possible to produce this martensitic transformation; this was first demonstrated by DeCarli and Jamieson (1961).

In light of this first shock synthesis, the long-known diamonds in iron meteorites and ureilites (Erofeev and Lachinov 1888, Foote 1891) were reinterpreted as shock products (Lipschutz 1964). On Earth, a large number of impact craters and the K/T boundary are yet known as find locations of impact diamonds (Masaitis et al. 1990 and 2000, Valter et al. 1992, Koeberl et al. 1997, Hough et al. 1997). They were first discovered in the 100 km sized Popigai structure, Siberia (Masaitis et al. 1972), which is regarded as largest diamond deposit on Earth (Deutsch et al. 2000). In the Ries, impact diamonds were already found in 1978 by Rost et al., but it was not before 1995 that this finding was noticed by a broader scientific community (Masaitis et al. 1995, Hough et al. 1995, El Goresy et al. 2001).

The source rocks of diamonds from terrestrial impact craters are usually graphite-bearing gneisses or other crystalline rocks (Masaitis et al. 1990, ElGoresy et al. 2001). Graphite in these rocks was transformed within the very short time of shock compression. As a consequence of the short transformation time, impact diamonds are very defect-rich and inherited some features of the precursor graphite. They are birefringent (Fig. 11a), retain the tabular hexagonal and sometimes even preserve spectacular growth twins rotated about the *c* axis of graphite (Fig. 11b). Therefore impact diamonds are regarded as para- or pseudomorphs after graphite and are called apographitic diamonds (Masaitis et al. 1990). At the TEM scale, these impact diamonds contain numerous kink or twin bands parallel to $(h\,h\,\overline{2h}\,l)$ planes of precursor graphite (Fig. 11c; Langenhorst et al. 1999b). The bands were generated
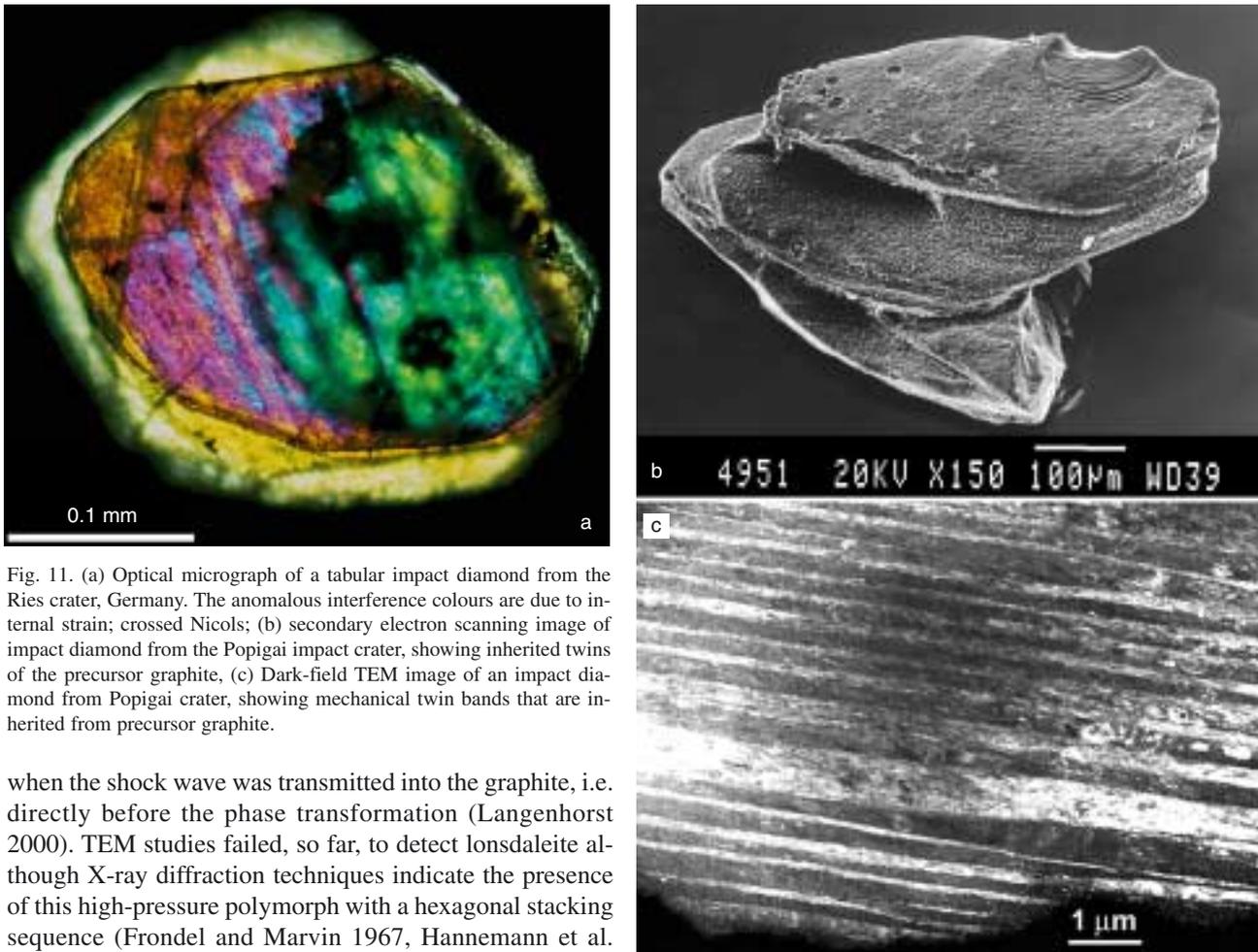
Fig. 11. (a) Optical micrograph of a tabular impact diamond from the Ries crater, Germany. The anomalous interference colours are due to internal strain; crossed Nicols; (b) secondary electron scanning image of impact diamond from the Popigai impact crater, showing inherited twins of the precursor graphite, (c) Dark-field TEM image of an impact diamond from Popigai crater, showing mechanical twin bands that are inherited from precursor graphite.

when the shock wave was transmitted into the graphite, i.e. directly before the phase transformation (Langenhorst 2000). TEM studies failed, so far, to detect lonsdaleite although X-ray diffraction techniques indicate the presence of this high-pressure polymorph with a hexagonal stacking sequence (Frondel and Marvin 1967, Hannemann et al. 1967, Masaitis et al. 1990). Instead, one observes that the diamonds are very disordered and contain numerous stacking faults, changing locally the cubic into a hexagonal stacking sequence (Langenhorst 2000). Diffuse X-ray scattering on these stacking faults is a way to explain the extra-peaks in X-ray diffraction patterns.

Strongly corroded impact diamonds that are intergrown with moissanite (SiC) have been found at the Ries impact crater, Germany. Based on this finding, Hough et al. (1995) concluded that the diamonds formed by vapour condensation (so-called chemical vapour deposition (CVD) mechanism). Meanwhile, this idea has been discarded, because the moissanite may have formed by reaction of diamond with silica-rich impact melt (Langenhorst et al. 1999b). This reaction also forms the basis for the industrial production of SiC (Mehrwald 1992). Incorporation of impact diamonds into hot impact melt additionally provides an elegant explanation for the corroded surfaces.

Calcite

Calcite possesses a crystal structure with planar CO_3 groups that are bridged via Ca atoms. The CO_3 groups are arranged in layers normal to the *c*-axis. The bonding between Ca cations and CO_3 groups is rather weak, allowing this structure to cleave as rhombohedra and to deform by mechanical twinning and dislocation glide (Nicolas and

Poirier 1976). Static deformation experiments have shown that calcite can basically develop three types of mechanical twins (Barber and Wenk 1979a): $e = \{01\bar{1}8\}$, $r = \{10\bar{1}4\}$ and $f = \{01\bar{1}2\}$ using the hexagonal unit cell setting with $a = 4.99$ Å and $c = 17.06$ Å. Little is known about the shock deformation of calcite but these twin laws apparently operate also under low to moderate shock pressures (Fig. 12a; Barber and Wenk 1979b, Langenhorst et al. 2002a). At slightly higher pressures, the microstructure of shocked calcite becomes more dominated by dislocations (Fig. 12b; Barber and Wenk 1976, Langenhorst et al. 2002a), occurring in a high density of up to 10^{14} m^{-2}. X-ray line broadening observed for naturally shocked calcite might be due to such high dislocation densities (Skála and Jakeš 1999).

Effects in the high-pressure regime are of fundamental importance, as calcite is known to decompose into solid CaO and gaseous CO_2. The devolatilization of carbonates by impacts is considered to be important for the evolution of Earth's atmosphere, climate, and life (Silver and Schultz 1980, Crutzen 1987). For example, the Chicxulub impact possibly perturbed the atmosphere with large amounts of CO_2 and SO_x, changing its radiative balance and causing acid rain (Emiliani et al. 1981, Prinn and Fegley 1987). This may have played an important role in the
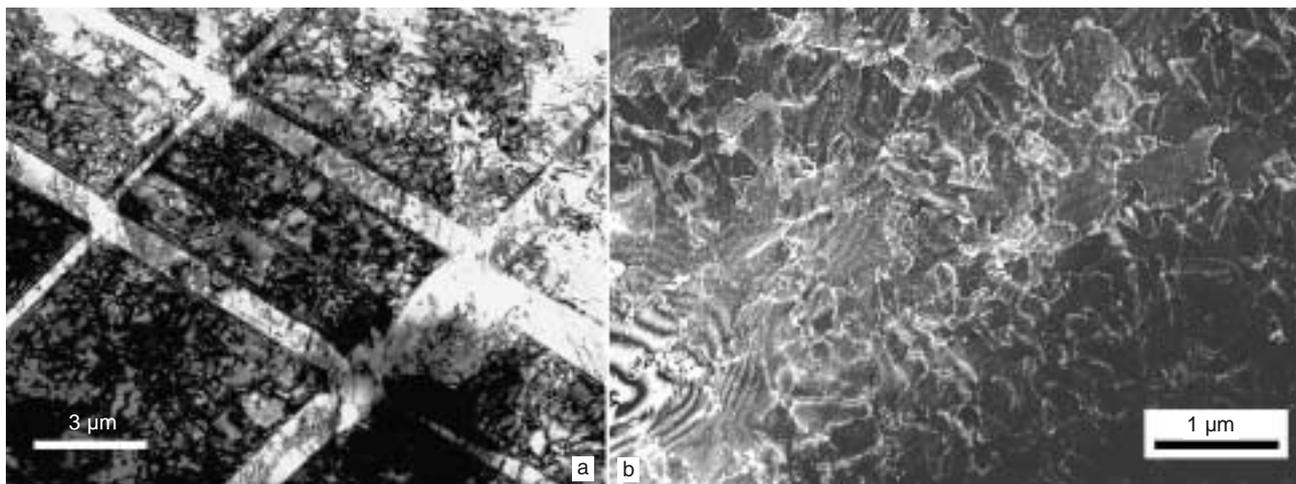
275

Fig. 12. Shock effects in calcite: (a) bright-field TEM image of crossing deformation twins in calcite shocked to 85 GPa using a high-explosive setup; (b) dark-field TEM image of numerous dislocations in a laser-shocked calcite (see Langenhorst et al. 2002a).

mass extinction scenario at the Cretaceous-Tertiary boundary (Alvarez et al. 1980).

Numerous shock experiments have recently been conducted to address the question of shock-induced devolatilization (Martinez et al. 1995, Skála et al. 2001, Ivanov et al. 2002, Langenhorst et al. 2002a). The experiments indicate that strongly shocked calcite can melt at high pressure but degassing probably takes only place after decompression if the post-shock temperatures are sufficiently high. This result is strengthened by theoretical calculations of the phase diagram of calcite (Ivanov and Deutsch 2002) and the discovery of quenched carbonate melts in suevites of the Ries and Chicxulub craters (Graup 1999, Jones et al. 2000). Furthermore, experiments indicate that back reactions between the decomposition products, CO_2 and CaO, are fast and efficient and therefore have to be taken into account in any quantification of impact-released CO_2 (Agrinier et al. 2001). To avoid the back reaction it is necessary to spatially separate the decomposition products, which is another complexity in a natural environment.

Shock-melted calcite develops upon quenching a feathery texture (Jones et al. 2000). Under the optical microscope, the feathery texture appears as aggregates of radiating, elongated calcite crystals. At the TEM scale, quench crystals of calcite are usually devoid of lattice defects, indicating that they went through the liquid state (Langenhorst et al. 2002a). On the other hand, incipient decomposition in shocked calcite is manifested by the presence of numerous tiny dislocation loops, indicative for the mobilization of CO_2 (Langenhorst et al. 2002a).

Estimation of shock conditions

A prerequisite for deciphering the shock-metamorphic history of minerals and their host rocks is an assessment of their pressure-temperature-time paths. It is important to re-

member here that polymict impact breccias consist of rock and mineral fragments that have suffered different degrees of shock metamorphism. Therefore it is necessary to consider each fragment separately.

The estimation of the shock duration is rather difficult, since no mineralogical speedometer is available. However, one can obtain a rough idea of the shock pulse if the size of the projectile is known from e.g. crater size. The shock pulse corresponds substantially to the time that the shock wave needs to propagate to the rear surface of the projectile and back to the point of impact.

The estimation of temperatures is a difficult task as well, because it is influenced by a number of factors such as porosity. In the context of shock metamorphism, one can, in principle, distinguish three different temperatures: (1) pre-shock, (2) shock and (3) post-shock temperatures. The pre-shock temperature is not directly related to shock metamorphism but elevated pre-shock temperatures have the effect to lower the threshold pressure for certain shock-metamorphic effects (Huffman et al. 1989, Langenhorst et al. 1992). It can be elevated due to regional metamorphism at the time of impact and the temperature could be determined via classical petrologic concepts (mineral assemblages, element partitioning between coexisting minerals). It is also known that PDF orientations in quartz significantly change at elevated pre-shock temperature, when quartz is shocked in the β high-temperature structure (> 573°C; Langenhorst and Deutsch 1994, Grieve et al. 1996). Quartz experimentally shocked in the β stability field contains PDFs parallel to planes of hexagonal pyramids, whereas shocked α-quartz exhibits PDFs that only belong to one rhombohedron (for further details see Langenhorst and Deutsch 1994).

Shock and post-shock temperatures are directly related to the magnitude of shock compression. The shock temperature is the maximum temperature achieved during shock compression, whereas the post-shock temperature is the temperature prevailing directly after decompression.

For compact materials, the pressure-dependence of shock and post-shock temperatures is fairly well known through calculations and pyrospectrometric measurements (e.g., Wackerle 1962, Raikes and Ahrens 1969, Martinez et al. 1995, Holland and Ahrens 1997; Fig. 5). Therefore, temperatures can be estimated from these reference data, if the shock pressure has been determined by applying a shock barometer.

It is more difficult to assess the shock and post-shock temperatures in porous rocks/minerals, because porosity has the general effect to significantly increase both temperatures. Shock compression leads however to compaction of rocks and loss of pore space, making it difficult to assess the initial porosity of rocks. Therefore, one can only apply simple arguments to estimate the temperatures from observations. For example, in case of mineral melting, the post-shock temperature has certainly exceeded the melting point of the mineral at ambient pressure.

The estimation of shock pressure relies on calibration data obtained in well-controlled shock experiments. Shock experiments have provided quantitative information on (1) co(existence) of shock effects in certain pressure ranges, (2) changes in physical (bulk) properties (e.g. refractive index and density), (3) variations in PDF orientations (Fig. 13), and (4) degree of mosaicism (Stöffler 1972, Stöffler et al. 1988, Hanns et al. 1978, Stöffler and Langenhorst 1994, Grieve et al. 1996, Langenhorst and Deutsch 1998).

To obtain a rough estimate of the shock pressure, it is often enough to use the petrographic microscope and to observe the shock effects in coexisting minerals. Data on the (co)existence of pressure-specific shock effects is available for most rock-forming minerals; compilations can be found in (Fig. 5): Stöffler (1972), Stöffler et al. (1988) and (1991), Bischoff and Stöffler (1992), Langenhorst and Deutsch (1998).

Better constraints on shock pressures can be obtained if the refractive indices or densities of quartz or feldspars were measured, using a spindle stage and a density gradient column (Fig. 13; Medenbach 1985, Langenhorst 1993). The change in these physical properties reflects the gradual conversion of quartz or feldspars into diaplectic glasses. This technique applies only over a small pressure range and requires that the glass is unaffected by post-shock annealing or alteration.

A more robust and widely used technique is to determine PDF orientations in quartz with an universal-stage (see appendix and Fig. 13, Stöffler and Langenhorst 1994, Grieve et al. 1996). Statistical data on PDF orientations in quartz have been provided, as a function of pressure, by various U-stage studies (Hörz 1968, Müller and Defourneaux 1969, Robertson and Grieve 1977, Langenhorst and Deutsch 1994). These measurements reveal, for example, that, at pressures of about 20 GPa, PDFs are predominantly oriented parallel to {10$\bar{1}$3} planes but change at higher pressure to {10$\bar{1}$2} orientations. A practical description on how to identify PDF orientations with an U-stage is given in the appendix of this paper.
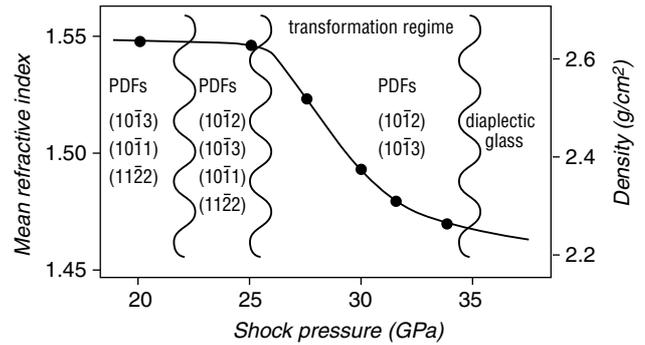

Fig. 13. Refractive index, density and combinations of PDF orientations of experimentally shocked quartz as function of pressure (from Langenhorst and Deutsch 1994).

X-ray diffractometer studies on shocked rock-forming minerals reveal an increasing degree of mosaicism with increasing shock pressure as expressed by decreasing diffraction peak amplitude and pronounced line-broadening (Hörz and Quaide 1973, Hanns et al. 1978). Although this technique is capable of yielding relatively accurate pressure determinations, it has never been widely applied because it requires fresh, unaltered samples.

Concluding remarks

In the past decade, we have made considerable progress in understanding the nature and formation mechanisms of shock effects in minerals. These advances are, to a large extent, due to TEM studies of shocked minerals, providing a thorough characterization of the defect microstructures.

Minerals show a unique response when subjected to strong shock waves. The effects range from deformation and transformation phenomena to decomposition, melting and vaporisation. Which shock effects are activated at what pressures and temperatures depends on the crystal structure and chemical composition of the mineral studied.

Most shock effects have been reproduced in short laboratory experiments with various designs, although the shock pulses in experiments can be more than 6 orders of magnitude shorter than those prevailing in nature. Experimental limits are however reached if more time-consuming processes are simulated, such as reconstructive phase transformations to high-pressure silicates. On the other hand, the experimental simulation is very successful in reproducing deformation defects in shocked minerals. Furthermore, experiments led also to a better understanding of post-shock modifications of mineralogical shock effects in the natural environment. Finally, the shock signature of minerals is not only an unequivocal indicator for hypervelocity impact but can also be used to obtain quantitative constraints on the pressures and temperatures in natural impacts.

References

Agrinier P., Deutsch A., Schärer U., Martinez I. (2001): Fast back-reactions of shock-released CO_2 from carbonates: an experimental approach. Geochim. Cosmochim. Acta, 65, 2615–2632.

Ahrens T. J., Rosenberg J. T. (1968): Shock metamorphism: experiments on quartz and plagioclase. In: French B. M., Short N. M. (eds) Shock metamorphism of natural materials, Mono Book Corp., Baltimore, pp. 59–81.

Ahrens T. J., Tsay F. D., Live D. H. (1976): Shock-induced fine-grained recrystallisation of olivine: Evidence against subsolidus reduction of Fe^{2+}. Proc. Lunar Sci. Conf. 7th, 1143–1156.

Alvarez L. W., Alvarez W., Asaro F., Michel H. V. (1980): Extraterrestrial cause for the Cretaceous-Tertiary extinction. Science, 208, 1095–1108.

Asay J. R., Shahinpoor M. (1993): High-Pressure Shock Compression of Solids. Spinger, New York, Berlin, Heidelberg.

Ashworth J. R., Barber D. J. (1975): Electron petrography of shock-deformed olivine in stony meteorites. Earth Planet. Sci. Lett., 27, 43–50.

Ashworth J. R., Schneider H. (1985): Deformation and transformation in experimentally shock-loaded quartz. Phys. Chem. Min., 11, 241–249.

Bauer J. F. (1979): Experimental shock metamorphism of mono- and polycrystalline olivine: A comparative study. Proc. Lunar Planet. Science Lett. 10th, 2573–2576.

Barber D. J., Wenk H. R. (1976): Defects in deformed calcite and carbonate rocks. In: Wenk H.-R. (ed.) Electron Microscopy in Mineralogy. Spinger, Berlin Heidelberg, New York, pp. 428–442.

Barber D. J., Wenk H. R. (1979a): Deformation twinning in calcite, dolomite, and other rhombohedral carbonates. Phys. Chem. Min., 5, 141–165.

Barber D. J., Wenk H. R. (1979b): On geological aspects of calcite microstructure. Tectonophysics, 54, 45–60.

Barker L. M., Shahinpoor M., Chhabildas L. C. (1993): Experimental and diagnostic techniques. In: Asay J. R. and Shahinpoor M. (eds) High-Pressure Shock Compression of Solids, Springer, New York, Berlin, Heidelberg, pp. 43–74.

Binns R. A., Davis R. J., Reed S. J. B. (1969): Ringwoodite, natural $(Mg,Fe)_2SiO_4$ spinel in the Tenham meteorite. Nature, 221, 943–944.

Bischoff A., Stöffler D. (1984): Chemical and structural changes induced by thermal annealing of shocked feldspar inclusions in impact melt rocks from Lappajärvi crater, Finland. J. Geophys. Res., 89, B645–B645.

Bischoff A., Stöffler D. (1992): Shock metamorphism as a fundamental process in the evolution of planetary bodies: Information from meteorites. Eur. J. Mineral., 4, 707–755.

Bloss F. D. (1961): An Introduction to the methods of optical crystallography. Holt, Rinehart and Winston, New York.

Bohor B. F., Foord E. E., Modreski P. J., Triplehorn D. M. (1984): Mineralogical evidence for an impact event at the Cretaceous-Teriary boundary. Science, 224, 867–869.

Bohor B. F., Modreski P. J., Foord E. E. (1987): Shocked quartz in the Cretaceous/Tertiary boundary clays: Evidence for global distribution. Science, 236, 705–708.

Boslough M. B., Asay J. R. (1993): Basic principles of shock compression. In: Asay J. R., Shahinpoor M. (eds) High-Pressure Shock Compression of Solids. Springer, New York, Berlin, Heidelberg, pp. 7–42.

Boslough M. B., Cygan R. T., Kirkpatrick R. J., Montez B. (1989): NMR spectroscopic analysis of experimentally shocked quartz and the formation of diaplectic glass. Lunar Planet. Science Conf. 20, 97.

Bourret A., Hinze E., Hochheimer H. D. (1986): Twin structure in coesite studied by high resolution electron microscopy. Phys. Chem. Minerals, 13, 206–212.

Brown J. M., McQueen R. G. (1986): Phase transitions, Grüneisen parameter and elasticity for shocked iron between 77 GPa and 400 GPa. J. Geophys. Res., 91, 7485–7494.

Byerly G. R., Lowe D. R., Wooden J. L., Xie X. (2002): An Archean impact layer from the Pilbara and Kapvaal cratons. Science, 297, 1325–1327.

Carstens H. (1975): Thermal history of impact melt rocks in the Fennoscandian shield. Contrib. Mineral. Petrol., 50, 145–155.

Carter N. L., Raleigh C. B., DeCarli P. S. (1968): Deformation of olivine in stony meteorites. J. Geophys. Res., 73, 5439–5461.

Cauble R., Phillion D. W., Hoover T. J., Holmes N. C., Kilkenny J. D., Lee R. W. (1993): Demonstration of 0.75 Gbar planar shocks in X-ray driven colliding foils. Phys. Rev.Lett., 70, 4, 2102–2105.

Chapman C. R., Morrison D. (1994): Impacts on the earth by asteroids and comets: Assessing the hazard. Nature, 367, 33–40.

Chen M., Sharp T. G., ElGoresy A. E., Wopenka B., Xie X. (1996): The majorite-pyrope + magnesiowüstite assemblage: constraints on the history of shock veins in chondrites. Science, 271, 1570–1573.

Cordier P., Vrána S., Doukhan J. C. (1994): Shock metamorphism in quartz at Sevetin and Susice (Bohemia)? A TEM investigation. Meteoritics, 29, 98–99.

Crutzen P. J. (1987): Acid rain at the K/T boundary. Nature, 330, 108–109.

Dachille F., Gigl P., Simons P. Y. (1968): Experimental and analytical studies of crystalline damage useful for the recognition of impact structures. In: French B. M., Short N. M. (eds) Shock Metamorphism of Natural Materials, Mono Book Corp., Baltimore, pp. 555–570.

Davison L., Horie Y., Sekine T. (2002): High-pressure shock compression of solids V-shock chemistry with applications to meteorite impacts. Springer, New York, pp. 245.

DeCarli P. S., Jamieson J. C. (1961): Formation of diamond by explosive shock. Science, 133, 1821–1822.

Deutsch A., Langenhorst F. (1998): Mineralogy of astroblemes – terrestrial impact craters. In: Marfunin. A. S. (ed.) Advanced Mineralogy 3, Springer, Berlin, pp. 76–95.

Deutsch A., Masaitis V. L., Langenhorst F., Grieve R. A. F. (2000): Popigai, Siberia - well preserved giant impact structure, national treasury, and world's geological heritage. Episodes, 23, 3–11.

Duvall G. E., Fowles G. R. (1963): Shock waves. In: Bradley R. S. (ed.) High Pressure Physics and Chemistry 2, Academic Press Inc., London, New York, pp. 209–291.

El Goresy A., Dubrovinsky L., Sharp T. G., Saxena S. K., Chen M. (2000): A monoclinic post-stishovite polymorph of silica in the Shergotty meteorite. Science, 288, 1632–1634.

El Goresy, A., Gillet P., Chen M., Künstler F., Graup G., Stähle V. (2001): In situ discovery of shock-induced graphite-diamond phase transition in gneisses from the Ries crater, Germany. Amer. Miner., 86, 611–621.

Emiliani C., Kraus E. B., Shoemaker E. M. (1981): Sudden death at the end of the Mesozoic. Earth Planet. Sci. Lett., 55, 317-334.

Emmons R. C. (1943): The universal stage. Geolog. Soc. Am., Mem. 8.

Engelhardt von W., Bertsch W. (1969): Shock induced planar deformation structures in quartz from the Ries crater, Germany. Contrib. Mineral. Petrol., 20, 203-234.

Engelhardt von W., Arndt J., Stöffler D., Müller W. F., Jeziorkowski H., Gubser R. A. (1967): Diaplektische Gläser in den Breccien des Ries von Nördlingen als Anzeichen für Stoßwellenmetamorphose. Contr. Miner. Petrol., 15, 93-102.

Erofeev M. V., Lachinov P. A. (1888): The description of the Novo Urey meteorite. Proceedings of the Emperor's Saint-Petersburg Mineralogical Society, pp. 13 (in Russian).

Ernstson K., Hammann W., Fiebag J., Graup G. (1985): Evidence of an impact origin for the Azuara structure (Spain). Earth Planet. Science Letters, 74, 361–370.

Federov von E. (1896): Universalmethode und Feldspathstudien. Zeits. Krist. Miner., 26, pp. 225.

Foote A. E. (1891): New locality for meteoritic iron with a preliminary notice of the discovery of diamonds in the iron. Amer. J. Sci, 42, 413–417.

French B. M. (1969): Distribution of shock-metamorphic features in the Sudbury Basin, Ontario, Canada. Meteoritics, 4, 173–174.

French B. M. (1998): Traces of catastrophe – A handbook of shock-metamorphic effects in terrestrial meteorite impact structures. LPI contribution No. 954, Lunar and Planetary Institute, Houston, 120 pp.

French B. M., Short N. M. (1968): Shock metamorphism of natural materials. Mono Book Corp, Baltimore, Maryland.

Frondel C., Marvin U. B. (1967): Lonsdaleite, a hexagonal polymorph of diamond. Nature, 214, 587–589.

Glass B. P., Liu S., Leavens P. B. (2002): Reidite: An impact-produced high-pressure polymorph of zircon found in marine sediments. Amer. Mineral., 87, 562–565.

Goltrant O., Cordier P., Doukhan J. C. (1991): Planar deformation features in shocked quartz: a transmission electron microscopy investigation. Earth Planet. Sci. Letters, 106, 103–115.

Goltrant O., Leroux H., Doukhan J.C., Cordier P. (1992): Formation mechanism of planar deformation features in naturally shocked quartz. Phys. Earth Planet. Int., 74, 219–240.

Gratz A. J., Nellis W. J., Christie J. M., Brocious W., Swegle J., Cordier P. (1992): Shock metamorphism of quartz with initial temperatures −170 to +1000°C. Phys. Chem. Miner., 19, 267–288.

Graup G. (1999): Carbonate-silicate liquid immiscibility upon impact melting: Ries crater, Germany. Meteoritics & Planetary Science, 34, 425–438.

Grieve R. A. F., Sharpton V. L., Stöffler D. (1990): Shocked minerals and the K/T controversy. EOS, 71, 1792–1793.

Grieve R. A. F., Shoemaker E. M. (1994): The record of past impacts on earth. In: Gehrels T. (ed.) Hazards due to comets and asteroids. Univ. of Arizona Press, Tucson, AZ, London, pp. 417–462.

Grieve R. A. F., Langenhorst F., Stöffler D. (1996): Shock metamorphism of quartz in nature and experiment: II. Significance in geoscience. Meteoritics & Planet. Sci., 31, 6–35.

Hannemann R. E., Strong H. M., Bundy F. P. (1967): Hexagonal diamonds in meteorites: implications. Science, 155, 995–997.

Hanns R. E., Montague B. R., Davis M. K., Galindo C., Hörz F. (1978): X-ray diffractometer studies of shocked materials. Proc. Lunar Planet. Sci., Conf. 9th, 2773–2787.

Hildebrand A. R., Penfield G. T., Kring D. A., Pilkington M., Camargo A. Z., Jacobsen S. B., Boyton W. V. (1991): Chicxulub crater: A possible Cretaceous/Tertiary boundary impact crater on the Yucatan Peninsula, Mexico. Geology, 19, 867–871.

Holland K. G., Ahrens T. J. (1997): Melting of $(Mg,Fe)_2SiO_4$ at the core-mantle boundary of the earth. Science, 275, 1623–1625.

Hornemann U., Müller W. F. (1971): Shock-induced deformation twins in clinopyroxene. Neues Jb. Mineral. Mh., 6, 247–256.

Hörz F. (1965): Untersuchungen an Riesgläsern. Beiträge Mineral. Petrographie, 11, 621–661.

Hörz F. (1968): Statistical measurements of deformation structures and refractive indices in experimentally shock-loaded quartz. In: French B. M., Short N. M. (eds) Shock metamorphism of natural materials. Mono Book Corp, Baltimore, Maryland, pp. 243–254.

Hörz F., Quaide W. L. (1973): Debye-Scherrer investigations of experimentally shocked silicates. The Moon, 6, 45–82.

Hough R. M., Gilmour I., Pillinger C. T., Arden J. W., Gilkes K. W. R., Yuan J., Milledge H. J. (1995): Diamond and silicon carbide in impact melt rock from the Ries impact crater. Nature, 378, 41–44.

Hough R. M., Pillinger C. T., Gilmour I., Langenhorst F., Montanari A. (1997): Diamonds from the iridium rich K-T boundary layer at Arroyo el Mimbral, Tamaulipas, Mexico. Geology, 11, 1019–1022.

Huffman A. R., Brown J. M., Carter N. L. (1989): Temperature dependence of shock-induced microstructures in tectosilicates. In: Schmidt S. C., Johnson J. N., Davison L. W. (eds) Shock Compression of Condensed Matter. Elsevier Science Publishers B.V., Amsterdam, pp. 649–652.

Ivanov B. A., Deutsch A. (2002): The phase diagram of $CaCO_3$ in relation to shock compression and decomposition. Phys. Earth Planet. Interiors, 129, 131–143.

Ivanov B. A., Langenhorst F., Deutsch A., Hornemann U. (2002): How strong was the impact-induced CO_2 degassing in the K/T event? Numerical modeling of laboratory experiments. In: Koeberl Ch., Mac Leod K. G. (eds) Catastrophic events and Mass Extinctions: Impact and beyond. Geol. Soc. Amer. Spec. Pap., 356, pp. 587–594.

Jackson I., Ahrens T. J. (1979): Shock wave compression of single-crystal forsterite. J. Geophys. Res., 84, 3039–3048.

Jeanloz R. (1980): Shock effects in olivine and implications for Hugoniot data. J. Geophys. Res., 85, 3163–3176.

Jeanloz R., Ahrens T. J., Lally J. S., Nord G. L., Christie J. M., Heuer A. H. (1977): Shock-produced olivine glass: First observation. Science, 197, 457–459.

Jones A. P., Claeys P., Heuschkel S. (2000): Impact melting of carbonates from the Chicxulub Crater. In: Gilmour I., Koeberl C. (eds) Impacts and the early Earth, Lecture Notes in Earth Sciences 91, Springer, Berlin-Heidelberg-New York, pp. 343–361.

Joreau P., Reimold W. U., Robb L. J., Doukhan J. C. (1997a): A TEM study of deformed quartz grains from volcaniclastic sediments associated with the Bushveld Complex, South Africa. Eur. J. Mineral., 9, 393–401.

Joreau P., Leroux H., Doukhan J. C. (1997b): A transmission electron microscope investigation of shock metamorphism in olivine of the Ilafegh 013 chondrite. Meteoritics & Planetary Sci., 32, 309–316.

Kieffer S. W., Phakey P. P., Christie J. M. (1976): Shock processes in porous quartzite: transmission electron microscope observations and theory. Contrib. Mineral. Petrol., 59, 41–93.

Koeberl C., Masaitis V. L., Shafranovsky G. I., Gilmour I., Langenhorst F., Schrauder M. (1997): Diamonds from the Popigai impact structure, Russia. Geology, 25, 967–970.

Lally J. S., Christie J. M., Nord G. L., Heuer A. H. (1976): Deformation, recovery and recrystallization of lunar dunite 72417. Proc. Lunar Sci. Conf. 7th, 1845–1863.

Langenhorst F., Deutsch A., Hornemann U., Stöffler D. (1992): Effect of temperature on shock metamorphism of single crystal quartz. Nature, 356, 507–509.

Langenhorst F. (1993): Eine modifizierte Dichtegradientenkolonne zur präzisen Dichtebestimmung an Einzelkörnern. Ber. Dtsch. Mineral. Ges. 1, Beih Eur. J. Mineral., 5, 244.

Langenhorst F. (1994): Shock experiments on α- and β- quartz: II. X-ray investigations. Earth Planet. Sci. Letters, 128, 638–698.

Langenhorst F. (1996): Characteristics of shocked quartz in late Eocene impact ejecta from Massignano (Ancona, Italy): Clues to shock conditions and source crater. Geology, 24, 487–490.

Langenhorst F. (2000): Stoßwellenmetamorphose von Mineralen: Neue Erkenntnisse durch Transmissionselektronenmikroskopie. Habilitation thesis, University of Bayreuth, Germany.

Langenhorst F., Deutsch A. (1994): Shock experiments on pre-heated α- and β- quartz: I. Optical and density data, Earth Planet. Science Letters, 125, 407–420.

Langenhorst F., Deutsch A. (1996): The Azuara and Rubielos structures, Spain; twin impact craters or alpine thrust systems? TEM investigations on deformed quartz disprove shock origin. Lunar Planet. Science Conf. 27, 725–726.

Langenhorst F., Deutsch A. (1998): Minerals in terrestrial impact structures and their characteristic features. In: Marfunin A. S. (ed.) Advanced Mineralogy 3, Springer, Berlin, pp. 95–119.

Langenhorst F., Greshake A. (1999): A TEM study of Chassigny: evidence for strong shock metamorphism. Meteoritics Planet. Sci., 34, 43–48.

Langenhorst F., Poirier J. P. (2000): Anatomy of black veins in Zagami: Clues to the formation of high-pressure phases. Earth Planet. Sci. Lett., 184, 37–55.

Langenhorst F., Poirier J. P. (2002): Transmission electron microscopy of coesite inclusions in the Dora Maira high-pressure metamorphic pyrope-quartzite. Earth Planet. Sci. Lett., 203, 793–803.

Langenhorst F., Joreau P. Doukhan J. C. (1995): Thermal and shock metamorphism of the Tenham meteorite: a TEM examination. Geochim. Cosmochim. Acta, 59, 1835–1845.

Langenhorst F., Boustie M., Migault A., Romain J. P. (1999a): Laser shock experiments with nanoseconds pulses: A new tool for the reproduction of shock defects in olivine. Earth Planet. Sci. Lett., 173, 333–342.

Langenhorst F., Shafranovsky G. I., Masaitis V. L., Koivisto M. (1999b): Discovery of impact diamonds in a Fennoscandian crater and evidence for their genesis by solid-state transformation. Geology, 27, 747–750.

Langenhorst F., Boustie M., Deutsch A., Hornemann U., Matignon Ch., Migault A., Romain J. P. (2002a): Experimental techniques for the simulation of shock metamorphism: A case study on calcite. In: Davison L., Horie Y., Sekine T. (eds) High-pressure shock compression of solids V-Shock chemistry with applications to meteorite impacts. Springer, New York, pp. 1–27.

Langenhorst F., Poirier J.-P., Deutsch A., Hornemann U. (2002b): Experimental approach to generate shock veins in single-crystal olivine by shear melting. Meteoritics & Planet. Sci., 37, 1541–1554.

Leroux H. (2001): Microstructural shock signatures of major minerals in meteorites. Eur. J. Mineral., 13, 253–272.

Leroux H., Doukhan J.-C. (1996): A transmission electron microscope study of shocked quartz from the Manson impact structure. Geol. Soc. Am. Spec. Paper, 302, 267–274.

Leroux H., Reimold W. U., Doukhan J. C. (1994): A TEM investigation of shock metamorphism in quartz from the Vredefort dome, South Africa. Tectonophysics, 230, 223–239.

Leroux H., Doukhan J. C., Guyot F. (1996): An analytical electron microscopy (AEM) investigation of opaque inclusions in some type 6 ordinary chondrites. Meteoritics & Planetary Sci., 31, 767–776.

Lipschutz M. E. (1964): Origin of diamonds in the Ureilites. Science, 143, 1431–1434.

Madon M., Poirier J. P. (1983): Transmission electron microscope observation of α, β and γ (Mg,Fe)$_2$SiO$_4$ in shocked meteorites: planar defects and polymorphic transitions. Phys. Earth Planet. Int., 33, 31–44.

Marsh S. P. (1980): LASL Shock Hugoniot Data. University of California Press, Berkeley, California.

Martinez I., Deutsch A., Schärer U., Ildefonse Ph., Guyot F., Agrinier P. (1995): Shock recovery experiments on dolomite and thermodynamical modeling of impact-induced decarbonation. J. Geophys Res., 100, B8, 15,465–15,476.

Martini J. E. J. (1991): The nature, distribution and genesis of the coesite and stishovite associated with the pseudotachylite of the Vredefort Dome, South Africa. Earth Planet. Sci. Letters, 103, 285–300.

Masaitis V. L., Futergendler D. I., Gnevushev M. A. (1972): Diamonds in impactites of the Popigay meteorite crater. Zap. Vsesoyuznogo Mineralogicheskogo Obshchestva 101, 108–112.

Masaitis V. L., Shafranovsky G. I., Ezersky V. A., Reshetnyak N. B. (1990): Impact diamonds in ureilites and impactites. Meteoritika 49, 180–195.

Masaitis V. L., Shafranovsky G. I., Federova I. G. (1995): The apographitic impact diamonds from astroblemes Ries and Popigai. Proc. Russ. Min. Soc., 4, 12–18.

Masaitis V. L., Shafranovsky G. I., Grieve R. A. F., Langenhorst F., Peredery W. V., Therriault A. M., Balmasov E. L., Federova I. G. (2000): Discovery of impact diamonds in black Onaping suevites, Sudbury structure, Ontario, Canada. In: Dressler B. O., Sharpton V. L. (eds) Large meteorite impacts and planetary evolution II, Geol. Soc. Am. Spec. Paper, 339, pp. 317–321.

McLaren A. C. (1991): Transmission electron microscopy of minerals and rocks. Cambridge Univ. Press, Cambridge, U.K.

McLaren A. C., Pithkethly D. R. (1982): The twinning microstructure and growth of amethyst quartz. Phys. Chem. Minerals, 8, 128–135.

McLaren A. C., Retchford J. A., Griggs D. T., Christie J. M. (1967): Transmission electron microscope study of Brazil twins and dislocations experimentally produced in natural quartz. Phys. Status Solidi, 19, 631–644.

Medenbach O. (1985): A new microrefractometer spindle stage and its application. Fortschritte Miner., 63, 111–133.

Mehrwald K.-H. (1992): History and economic aspects of industrial SiC manufacture. Berichte der Deutschen Keramischen Gesellschaft, 69, 72–81.

Melosh H. J. (1989): Impact cratering – A geological process. Oxford Univ. Press, New York.

Milton D. J., DeCarli P. S. (1963): Maskelynite: formation by explosive shock. Science, 140, 670–671.

Müller W. F. (1969): Elektronenmikroskopischer Nachweis amorpher Bereiche in stoßwellenbeanspruchtem Quarz. Naturwiss., 56, 279.

Müller W. F., Defourneaux W. (1969): Deformationsstrukturen in Quarz als Indikator für Stoßwellen: eine experimentelle Untersuchung an Quarzeinkristallen. Z. Geophys., 34, 483–504.

Müller W. F., Hornemann U. (1969): Shock-induced planar deformation structures in experimentally shock-loaded olivines and in olivines from chondritic meteorites. Earth Planet. Sci. Letters, 7, 251–264.

Neukum G., Ivanov B. A., Hartmann W. K. (2001): Cratering records in the inner solar system in relation to the lunar reference system. Space Sci. Rev., 96, 55–86.

Nicolas A., Poirier J. P. (1976): Crystalline plasticity and solid state flow in metamorphic rocks. Wiley, New York, 444 pp.

Nicolaysen L. O., Reimold W. U. (1990): Cryptoexplosions and Catastrophes in the Geological Record, with a special focus on the Vredefort structure. Tectonophysics, 171, pp. 422.

Nikitin W. W. (1936): Die Federow-Methode. Borntraeger, Berlin, pp. 109.

Phillips W. R. (1971) Mineral optics – principles and techniques. Freeman, San Francisco, pp. 249.

Poirier J. P. (1985): Creep of crystals. Cambridge University Press, Cambridge.

Prinn R. G., Fegley B., Jr. (1987): Bolide impacts, acid rain and biospheric traumas at the Cretaceous-Tertiary boundary. Earth Planet. Sci. Lett., 83, 409–418.

Putnis A., Price G. D. (1979): High pressure (Mg,Fe)$_2$SiO$_4$ phases in the Tenham chondritic meteorite. Nature, 280, 217–218.

Raikes S. A., Ahrens T. J. (1979): Post-shock temperatures in minerals. Geophys. J. R. Astron. Soc., 58, 717–747.

Reimold W. U., Stöffler D. (1978): Experimental shock metamorphism of dunite. Proc. Lunar Planet. Sci. Lett. 9th, 2805–2824.

Reinhard M. (1931): Universal Drehtischmethoden. Verlag Von B. Wepf und Cie, Basel, pp. 119.

Robertson P. B., Grieve R. A. F. (1977): Shock attenuation at terrestrial impact structures. In: Roddy D. J., Pepin P. O., Merill R. B. (eds) Impact and explosion cratering. Pergamon Press, New York, pp. 687–702.

Robin E., Bonté Ph., Froget L., Jéhanno C., Rocchia R. (1992): Formation of spinels in cosmic objects during atmospheric entry: a clue to the Cretaceous-Tertiary boundary event. Earth Planet. Sci. Lett., 108, 181–190.

Roddy D. J., Pepin R. O., Merrill R. B. (1977): Impact and explosion cratering. Pergamon Press, New York, pp.1301.

Rost R., Dolgov Y., A., Vishnevskiy S., A. (1978): Gases in inclusions of impact glass in the Ries crater, West Germany, and finds of high-pressure carbon polymorphs. Doklady Akademii Nauk SSSR, 241, 165–168.

Rubie D. (1999): Characterising the sample enviroment in multianvil high-pressure experiments. Phase Transitions, 68, 431–451.

Schmitt R. T. (2000): Shock experiments with the H6 chondrite Kernouvé: pressure calibration of microscopic shock effects. Meteoritics & Planet. Sci., 35, 545–560.

Schneider H. (1978): Infrared Spectroscopic Studies of Experimentally Shock-Loaded Quartz. Meteoritics, 13, 227.

Schreyer W. (1983): Metamorphism and fluid inclusions in the basement of the Vredefort Dome, South Africa: Guidelines to the origin of the structure. J. Petrol., 24, 26–47.

Sharp T. G., Lingemann C. M., Dupas C., Stöffler D. (1997): Natural occurrence of MgSiO$_3$-ilmenite and evidence for MgSiO$_3$-perovskite in a shocked L chondrite. Science, 277, 352–355.

Sharp T. G., ElGoresy A., Wopenka B., Chen M. (1999): A post-stishovite SiO$_2$ polymorph in the meteorite Shergotty: implications for impact events. Science, 284, 1511–1513.

Silver L. T., Schultz P. H. (1982): Geological implications of impacts of large asteroids and comets on the Earth. Geol. Soc. Amer. Spec. Pap., 190, Boulder.

Skála R., Jakeš P. (1999): Shock-induced effects in natural calcite-rich targets as revealed by X-ray powder diffraction. Geol. Soc. Amer. Spec. Pap., 339, 205–214.

Skála R., Ederová J., Matějka P., Hörz F. (2001): Mineralogical studies of experimentally shocked dolomite: Implications for the outgassing

of carbonates. In: Koeberl Ch., Mac Leod K. G. (eds) Catastrophic events and Mass Extinctions: Impact and beyond. Geol. Soc. Amer. Spec. Pap., 356, pp. 571–586.

Snee L. W., Ahrens T. J. (1975): Shock induced deformation features in terrestrial peridot and lunar dunite. Proc. Lunar Planet. Sci. Conf. 6th, 833–842.

Stebbins J. F., Poe B. T. (1999): Pentacoordinate silicon in high-pressure crystalline and glassy phases of calcium disilicate (CaSi$_2$O$_5$). Geophys. Res. Lett., 26, 2521–2523.

Stöckhert B., Duyster J., Trepmann C., Massonne H.-J. (2001): Microdiamond daughter crystals precipitated from supercritical COH + silicate fluids included in garnet, Erzgebirge, Germany. Geology, 29, 391–394.

Stöffler D. (1971): Coesite and stishovite: Identification and formation conditions in shock-metamorphosed rocks. J. Geophys. Res., 76, 5474–5488.

Stöffler D. (1972): Deformation and transformation of rock-forming minerals by natural and experimental shock processes: I. Behaviour of minerals under shock compression. Fortschritte der Mineralogie, 49, 50–113.

Stöffler D. (1974): Deformation and transformation of rock-forming minerals by natural and experimental shock processes: II. Physical properties of shocked minerals. Fortschritte der Mineralogie, 51, 256–289.

Stöffler D. (1984): Glasses formed by hypervelocity impact. J. Non-Cryst. Solids, 67, 465–502.

Stöffler D., Langenhorst F. (1994): Shock metamorphism of quartz in nature and experiment: I. Basic observation and theory. Meteoritics, 29, 155–181.

Stöffler D., Ryder G. (2001): Stratigraphy and isotope ages of lunar geologic units: chronological standard for the inner solar system. Space Science Reviews, 96, 9–54.

Stöffler D., Bischoff A., Buchwald V., Rubin A.,E. (1988): Shock effects in meteorites. In: Kerridge J. F., Matthews M. S. (eds) Meteorites and the Early Solar System. Univ. of Arizona press, Tuscon, pp. 165–202.

Stöffler D., Keil K., Scott E. R. D. (1991): Shock metamorphism of ordinary chondrites. Geochim. Cosmochim. Acta, 55, 3845–3867.

Tomioka N., Fujino K. (1997): Natural (Mg,Fe)SiO$_3$-ilmenite and -perovskite in the Tenham meteorite. Science, 277, 1084–1086.

Valter A. A., Yeremenko G. K., Kwasnitsa V. N., Polkanov Y. A. (1992): Shock-metamorphosed carbon minerals. Nauka Press, Kiev (in Russian).

Vrána S. (1987): The Sevetin astrobleme, southern Bohemia, Czechoslovakia. Geol. Rundschau, 76, 505–528.

Wackerle J. (1962): Shock wave compression of quartz. J. Appl. Phys., 33, 922–937.

Walzebuck J. P., von Engelhardt W. (1979): Shock deformation of quartz influenced by grain size and shock direction: observations on quartz-plagioclase rocks from the basement of the Ries crater, Germany. Contr. Mineral. Petrol., 70, 267–271.

Wegener A. (1921): Die Entstehung der Mondkrater. Friedrich Vieweg & Sohn, Braunschweig, pp. 48.

Wetherill G. W. (1984): Accumulation of terrestrial planets and implications concerning lunar origin. In: Hartmann W. K., Phillips R. J., Taylor G. J. (eds) Origin of the Moon. Lunar and Planet. Sci. Inst., Houston, pp. 519–550.

White J. C. (1993): Shock-induced melting and silica polymorph formation, Vredefort structure, South Africa. In: Boland J. A., FitzGerald J. D. (eds) Defects and processes in solid state: geoscience applications. Elsevier, New York, pp. 69–84.

Xue X., Stebbins J. F., Kanzaki M., Trønnes R. G. (1989): Silicon coordination and speciation changes in a silicate liquid at high pressures. Science, 245, 962–964.

Handling editor: Roman Skála

APPENDIX: *How to determine PDF orientations ?*

The following is a simple description on how to determine the crystallographic orientation of PDFs in shocked quartz grains, using an universal stage (von Federov 1896, Reinhard 1931, Nikitin 1936, Emmons 1943, Phillips 1971). Although the use of universal stages has considerably declined in structural geology, it remains the only method, which provides statistical data on the orientation of PDFs. Other techniques such as TEM are also capable of measuring PDF orientations but TEM measurements are too time-consuming to obtain statistically meaningful data.

There are four fundamental practical steps in the determination of PDF orientations in shocked quartz. One has to locate the spatial orientation of *(1)* the optic axis (parallel to *c* axis) and *(2)* the normals to the PDF planes in the grain studied. Once these directions are known from measurements, they are plotted and transformed in a stereographic Wulff net *(3)* and can then be indexed by comparison with the standard stereographic projection of quartz *(4)*.

(1) Since quartz is an uniaxial (trigonal) mineral it is only possible to locate the *c* axis optically. The *a* axes are in the plane perpendicular to *c* but their exact positions within this plane are not measurable. This causes a problem for indexing a PDF plane because the angle to the *c* axis can be measured but not the angle to the *a* axes. To circumvent this problem in part one needs at least two or more crossing PDF sets in a single quartz grain. To explain on how to locate the *c* axis of quartz, we will follow here the Reinhard notation of rotation axes for a 4-axis or 5-axis universal stage (Reinhard 1931, Fig. 14). Depending on the orientation of the quartz grain studied, the optic axis can be brought either parallel to the M (microscope) axis or parallel to the K (control) axis (E-W). Hence the first step is to find out whether the optic axis of the quartz grain is highly inclined to (polar position) or lies almost within the plane (equatorial position) of the thin section.

Polar position: Rotate about the M axis to the diagonal position (45° to E-W) and then rotate about the H axis until the grain extincts under crossed Nicols. If it remains light, the grain is in the equatorial position

(see below). Rotate about the M axis to restore the 0° position, but keep H at its inclined position. The grain will become light again (unless the optic axis is already parallel to M). Now rotate about the N axis to achieve again the extinction position. Finally, repeat all the steps until the grain remains extinct when rotated about the M axis.

Equatorial position: Rotate first about the N axis until the quartz grain extincts and its optic axis is in the E-W plane. This is the case if the grain becomes light by a further rotation about the K axis. Rotate then about the H axis until the extinction position of the grain is restored. The grain will again become light by a further rotation about the K axis in opposite direction (unless the optic axis is already parallel to E-W). Finally, repeat all the steps until the grain remains extinct when tilted about the K axis. The equatorial position is the more common situation in PDF measurements, because PDF poles mostly form a small angle to the *c* axis.

(2) To determine the orientation of a PDF plane it is necessary to bring its normal parallel to E-W. This is achieved by rotating about the N axis until the trace of the PDF plane is parallel to N-S. Rotate then about the H axis until the trace becomes as sharp as possible. One can test whether the plane is exactly vertical by defocusing the PDF. It is vertical if the trace of the PDF does not move. Another way to test for the vertical position is to tilt about the K axis. If the PDF plane is exactly vertical, its trace will remain in N-S orientation.

(3) The two important rotation angles to be plotted in the stereonet are the azimuth angle (i.e. rotation about N) and the ρ angle (i.e. rotation about H). When plotting the values for the optic axis, it has to be remembered whether it was tilted vertically or horizontally. Additionally, one needs to keep in mind the sense of tilting about H. Detailed descriptions on the plotting of U-stage data can be found in Bloss (1961) and Phillips (1971). Once the orientation of the optic axis and the normals to PDF planes are plotted, they need to be transformed into the standard stereographic projection with the *c* axis in the center (Fig. 15). The pole of the optic axis is transformed along the equatorial line of the Wulff net toward the center, and the normals to
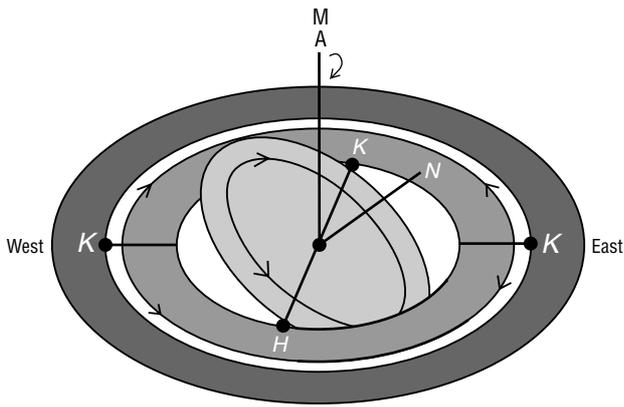
Fig. 14. Sketch of the rotation axes on a 5-axis universal stage. The notation of axes is according to Reinhard (1931): M = microscope axis, A = auxiliary axis, N = normal axis, H = horizontal axis, and K = control axis.

1 (0001)
2 {10$\bar{1}$3}
3 {10$\bar{1}$2}
4 {10$\bar{1}$1}
5 {10$\bar{1}$0}
6 {11$\bar{2}$2}
7 {11$\bar{2}$1}
8 {21$\bar{3}$1}
9 {51$\bar{6}$1}
10 {11$\bar{2}$0}

Fig. 16. Standard stereographic projection of quartz with the *c* axis in the center. The circles have a 5° radius and mark the positions of the most abundant PDF orientations (modified after Stöffler and Langenhorst 1994). Since quartz is trigonal, one can distinguish positive and negative (e.g., rhombohedra) as well as right and left (e.g. pyramids) forms.

' – transformed positions
OA – optic axis
FN – face normal
Δ – azimuth difference
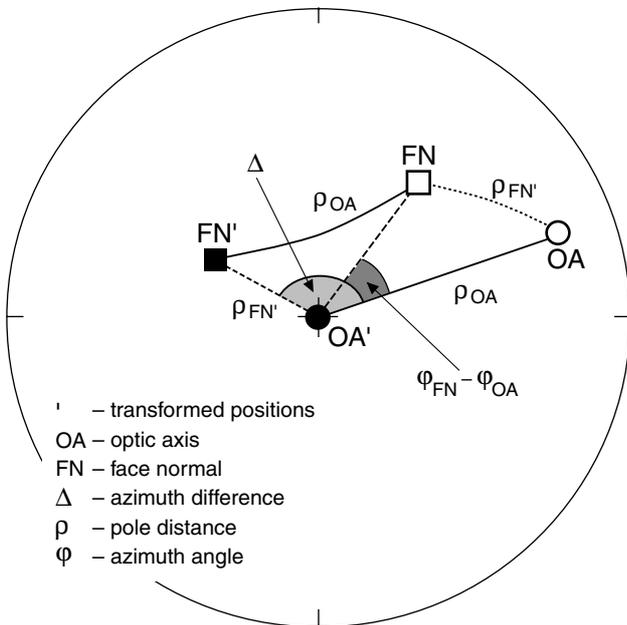ρ – pole distance
φ – azimuth angle

Fig. 15. An example for the transformation of a PDF pole (FN) and the optic axis (OA) into the standard stereographic projection of quartz with the optic axis (=*c* axis) in the center.

Fig. 17. Example for PDF orientations in quartz experimentally shocked to 25 GPa (from Langenhorst and Deutsch 1994). The right-hand diagram depicts schematically the full symmetry of coexisting forms.

the PDF planes are transformed along small circles by the same angle (see also von Engelhardt and Bertsch 1969). You can read now the angle between the PDF normals and the *c* axis. Alternatively, one can calculate this angle by the following equation:

$$\cos \rho_{FN'} = \cos \rho_{FN} \cos \rho_{OA} + \sin \rho_{FN} \sin \rho_{OA} \cos (\varphi_{FN} - \varphi_{OA}) \quad (5)$$

In the literature, one will often find histograms in which this angle is plotted as function of the frequency of PDFs. However, as the *a*-axes cannot be located by polarizing microscopy, the angle to the *c* axis alone is insufficient for unequivocal indexing of PDF planes. This problem cannot be solved if the quartz grain of interest contains only one set of PDFs. However, if the grain contains at least two sets of PDFs, the next analytical step probably yields a reliable indexing result.

(4) In this final step, the transformed stereoplot is compared to the standard stereographic projection of quartz, displaying the orientation of known PDF planes (Fig. 16). The latter are drawn as 5° circles, rep-
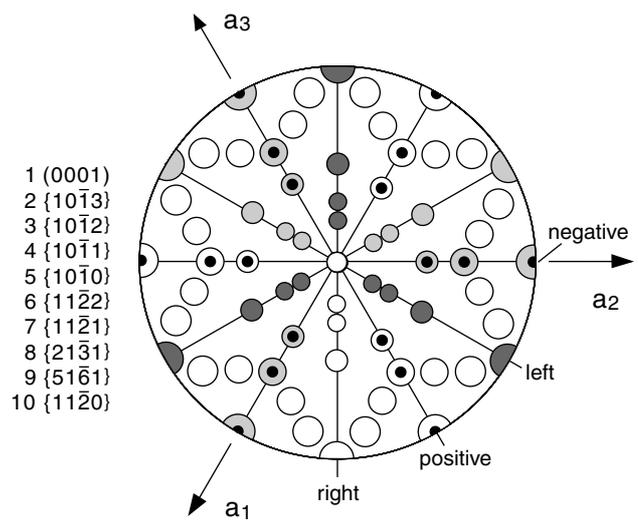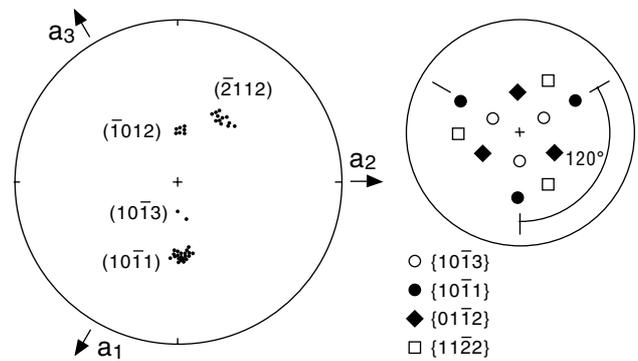
resenting the estimated errors in the measurements. Table 1 shows that not only the pole distance varies for the crystallographic PDF planes but also the azimuth angles, e.g. rhombedral forms lie 30° off the pyramidal forms because they do not belong to the same crystallographic zone. This is the basis for indexing the PDF planes. In practice, the stereographic projection of measured PDF poles is rotated until all poles fall into the circles of the standard stereographic projection (Fig. 16). Usually, there should be only one indexing solution; if the measurements are not precise enough, some PDFs can remain unindexed. The stereographic projection yields not only the Miller indices of PDF planes but also provides information on the coexistence of positive and negative or right and left forms (Langenhorst and Deutsch 1994). Figure 17 shows an example for typical PDF combinations in quartz shocked at a pressure of 25 GPa. It demonstrates that the positive rhombohedra {10$\bar{1}$1} and {10$\bar{1}$3} are combined with the negative rhombohedron {01$\bar{1}$2} and the right pyramid {11$\bar{2}$2}. It is of course not possible to distinguish between a negative and a positive form but when indexing a stereogram one has to make an arbitrary choice for the first PDF pole (positive or negative) and can then consistently index the following poles.